universität wien

MASTERARBEIT / MASTER'S THESIS

Titel der Masterarbeit / Title of the Master´s Thesis

„The ontogeny of hominid cranial form: A geometric morphometric analysis of coordinated and compensatory processes“

verfasst von / submitted by

Silvester Bartsch, BSc

angestrebter akademischer Grad / in partial fulfilment of the requirements for the degree of

Master of Science (MSc)

Wien, 2019 / Vienna, 2019

Studienkennzahl lt. Studienblatt / degree programme code as it appears on the student record sheet:	UA 066 827
Studienrichtung lt. Studienblatt / degree programme as it appears on the student record sheet:	Masterstudium Anthropologie
Betreut von / Supervisor:	Assoz. Prof. Mag. Dr. Philipp Mitteroecker
Mitbetreut von / Co-Supervisor:	Nicole Grunstra, BA MSc PhD

Contents

Acknowledgements

I would like to thank my supervisor Assoz. Prof. Mag. Dr. Philipp Mitteroecker for giving me the opportunity to start an internship at the Department of theoretical Biology and work with him on this thesis, for his most helpful input, his patience in teaching me statistics and the support in preparation for conferences that we have attended while working on this project. Also, I would like to thank Dr. Nicole Grunstra for co-supervision of this thesis. The afternoons we spent while deriving an appropriate landmark scheme and searching the NHM and online-databases for specimens, as well as the constant discussion of incoming results have made this project a joy to work on. In addition, I would like to thank Dr. Anne Le-Maitre for her help in programming in R, Univ. Prof. Dr. Gerhard Weber and Mag. Martin Dockner for their great help in scanning specimens in the Vienna μCT-Lab and Prof. Dr. habil. Frank Zachos for access to specimens of the Mammal collection at the Natural History Museum of Vienna. I also thank Christine Hemm for access to specimens from the Senckenberg Naturmuseum Frankfurt.

Abstract

The cranium is a highly functional morphological complex in vertebrates: It protects and houses the brain, the sensory organs and the masticatory apparatus. Individual cranial bones need to form an integrated whole in order to facilitate these functions throughout development and into adulthood, in spite of the considerable changes in cranial shape that are taking place during ontogeny. Previous studies on these developmental interactions used the concept of modularity, i.e. the complete independence of traits which manifests itself in a covariance of 0, as a null model, the deviations from which are not always adequately interpretable in a morphometric context. A novel theoretical framework introduced the null-model of self-similarity, interpreted as a state where independent developmental processes underlie the morphology of traits. Deviations from this null-model can be interpreted as either a dominance of coordinated or compensatory growth processes during ontogeny. I use this approach for a novel study of human and chimpanzee cranial shape by decomposing it into two components: The 'global' component reflects the functionally relevant features of cranial shape and captures large-scale morphological variation, which is represented by the cranial outline. The 'local' component or 'residual' shape, which captures more small-scale variation, represents the relative contribution of individual bones to overall shape. This approach allows me to investigate the extent to which postnatal ontogenetic changes in cranial shape occur in the overall shape versus the relative contribution of individual bones, respectively.

My thesis aims to investigate possible differences in the kind of growth process (coordinated or compensatory growth) leading to adult cranial form in *Pan troglodytes* and *Homo sapiens*, with an additional focus as to whether these processes have different effects on the chondrocranium and the desmocranium. Furthermore, my study addresses whether differences in the contribution of bones to overall cranial shape contribute to the apparent differences in cranial shape between the two species.

To this end, a set of 93 midsagittal landmarks, which captures classical anatomical landmarks, as well as the delineations of individual cranial bones, was devised. The landmarks were measured on 84 CT-scanned crania of different age classes and a geometric morphometric analysis was conducted.

The results revealed that the ontogeny of cranial size is mainly driven by coordinated growth processes in both species. On the other hand, the ontogeny of cranial shape is mostly driven by compensatory growth processes in both humans and chimpanzees. No clear answer

as to whether coordinated or compensatory growth processes dominate over the development of the chimpanzee desmocranium was found. In the comparison of global and local aspects of cranial shape, a principal component analysis (PCA) of outline shape showed species differences as well as ontogenetic trajectories, which were similar for humans and chimpanzees. By contrast, a PCA of residual shape showed no ontogenetic trend within either species. Interspecific differences were less pronounced although they remained statistically significant.

These findings indicate that two distinct processes underlie cranial development in chimpanzees and humans. Most likely, these processes have evolved to buffer developmental perturbations and to ensure the functional integrity of the cranium. The coordinated growth of cranial size likely is accomplished through the expression of growth factors with pleiotropic effects in several cranial regions as well as epigenetic effects, such as the influence of brain growth on calvarial size. In terms of cranial shape, *intraspecific differences* in cranial shape presumably are accomplished via epigenetic mechanisms, such as the "bone mechanostat", which monitors physical strains on developing and remodelling bone tissue. However, *interspecific differences* in cranial shape may have arisen through epigenetic mechanisms which have eventually manifested themselves in complex genetic networks that require further investigation.

In addition, it was found that postnatal development of cranial shape is accrued via global, rather than local shape changes. The contribution of bones to the overall cranium is largely determined prenatally, perhaps even in the cartilaginous precursors of bones, and remains largely stable during postnatal development. This finding may indicate that overall cranial shape is functionally more relevant than residual cranial shape, opening new possibilities for morphology-based phylogenetic reconstruction.

Zusammenfassung

Der knöcherne Schädel vertebrater Organismen stellt eine höchst funktionelle Struktur dar: Er umfasst und schützt das Gehirn, diverse Sinnesorgane sowie den Kauapparat. Die einzelnen Schädelknochen müssen in integrativer Weise wachsen, um diese Funktionen während der Entwicklung und im erwachsenen Organismus, trotz der wichtigen morphologischen Veränderungen in der Ontogenie, sicherzustellen. Frühere Studien haben dieses Zusammenspiel unter dem Gesichtspunkt der Modularität, der vollständigen Unabhängigkeit einzelner Merkmale, erforscht, obwohl sich dieses Konzept in einem morphometrischen Kontext nur selten als biologisch interpretierbar erweist. Das theoretische Konzept der „self-similarity“, die aus entwicklungsbiologischen Unabhängigkeiten oder einer gegenseitigen Aufhebung von positiv und negativ korrelierten Effekten zwischen Merkmalen entsteht, wird in dieser Studie als alternatives Nullmodell angewandt. Abweichungen von diesem Nullmodell erlauben es, zwischen koordinierten und kompensatorischen Vorgängen während der Ontogenie zu unterscheiden. Diese Arbeit präsentiert außerdem einen neuen konzeptionellen Ansatz, in dem das Cranium in zwei Komponenten unterteilt wird: Die „globale“ Komponente repräsentiert die äußere Schädelgestalt und erfasst damit großräumige Gestaltvariation. Die „lokale“ Komponente, auch „residual shape“ genannt, repräsentiert die Knochenzusammensetzung anatomischer Strukturen und erfasst somit kleinräumige Gestaltvariation. Dieser Ansatz ermöglicht die Erfassung des Ausmaßes, in welchem postnatale ontogenetische Prozesse die generelle Schädelgestalt und den relativen Beitrag von Knochen zu anatomischen Strukturen verändern.

Die Arbeit wird mögliche Unterschiede in der Art der Wachstumsprozesse (koordiniert oder kompensatorisch), die zur adulten Schädelform von *Pan troglodytes* und *Homo sapiens* führen, untersuchen. Im Speziellen wird auf die Frage, ob diese Prozesse im Chondrocranium und im Desmocranium unterschiedlich stark ausgeprägt sind, eingegangen. Außerdem wird der Frage nachgegangen, ob Unterschiede in der Knochenzusammensetzung cranialer Strukturen zu interspezifischen Unterschieden der äußeren Schädelgestalt beitragen.

Hierzu wurde ein Set aus 93 median-sagittal gesetzten Landmarks, die sowohl die äußere Schädelgestalt, als auch Knochengrenzen erfassen, entwickelt. Die Landmarks wurden auf 84 CT-Scans von Schädeln nicht-adulter sowie adulter Individuen gesetzt und anschließend mit den Methoden der sogenannten „geometric morphometrics“ analysiert.

Sowohl die Messungen an menschlichen Schädeln, als auch an jenen der Schimpansen, zeigen, dass die craniale Größenentwicklung von koordinierten Wachstumsprozessen geprägt ist, während in der Gestaltentwicklung kompensatorische Prozesse überwiegen. Im Fall des Schimpansen konnte kein Schluss in der Frage, ob koordinierte oder kompensatorische Prozesse überwiegen, gezogen werden- hier wurden deshalb auch die größten interspezifischen Unterschiede gefunden. Beim Vergleich der Entwicklung in der globalen und lokalen Komponente des Craniums zeigte eine Hauptkomponentenanalyse der äußeren Schädelgestalt sowohl eine ontogenetische Trajektorie, als auch interspezifische Unterschiede auf. Im Gegensatz dazu ergab eine Hauptkomponentenanalyse der lokalen Gestaltkomponente keine ontogenetischen Veränderungen. Interspezifische Unterschiede waren gering, erwiesen sie sich jedoch als statistisch signifikant.

Diese Ergebnisse deuten auf zwei gegensätzliche Prozesse hin, die der Entwicklung des Schimpansen- und Menschenschädel unterliegen. Höchstwahrscheinlich haben sich diese Mechanismen als Reaktion auf Störungen während der Entwicklung etabliert, um die funktionellen Anforderungen des Craniums sicherzustellen. Die koordinierte Entwicklung der Schädelgröße wird durch die Expression von Wachstumsfaktoren mit pleiotropischen Effekten in einer Reihe von cranialen Strukturen, sowie durch epigenetische Prozesse, wie dem Einfluss des Hirnwachstums auf das Wachstum der Schädeldecke, bewerkstelligt. *Intraspezifische* Unterschiede in der Schädelgestalt entstehen durch epigenetische Prozesse, wie dem sogenannten „bone mechanostat“, der die mechanischen Ansprüche der Knochen kontrolliert und Knochengewebe gegebenenfalls remodelliert. *Interspezifische* Unterschiede der Schädelgestalt haben höchstwahrscheinlich in epigenetischen Prozesse, die sich in komplexen genetischen Netzwerken manifestiert haben, ihren Ursprung. Hierzu bedarf es jedoch weiterer Untersuchungen.

Außerdem konnte gezeigt werden, dass die postnatale Entwicklung der Schädelgestalt auf großräumigen und nicht auf kleinräumigen Veränderungen beruht. Die Knochenzusammensetzung anatomischer Strukturen ist pränatal, in knorpeligen Vorläufern der Knochen, festgelegt und verändert sich während der postnatalen Entwicklung kaum. Möglicherweise folgt aus diesem Ergebnis, dass die äußere Schädelgestalt funktionell wichtiger als die Knochenzusammensetzung derselben ist. Diese Erkenntnis könnte wichtige neue Möglichkeiten für phylogenetische Rekonstruktionen, die auf morphologischen Daten beruhen, eröffnen.

Introduction

The ontogenetic processes leading to the morphology of the primate cranium, and its functional integrity, have been subject to extensive research over the last decades (Lieberman & McCarthy, 1999; Strait, 2001; Bookstein et al., 2003; Mitteroecker et al., 2004; Zelditch et al., 2004; Mitteroecker et al., 2005; Zelditch et al., 2006; Mitteroecker & Bookstein, 2008; Mitteroecker, 2009; Mitteroecker, 2012; Neaux, 2017; Scott et al., 2018). Most studies have focused on the analysis of the primate skull under the heading of "morphological integration". Ever since Olson and Miller (1958) coined the term *morphological integration*, there has been no universal definition of what is meant by it (Mitteroecker et al., 2012). The underlying idea, however, is that in order to develop an organismal structure, its different substructures have to be under some kind of common control and thus undergo a functionally and geometrically integrated evolution.

As a result of this insufficient definition, *morphological integration* has been used both as a term to interpret functional and developmental dependencies of biological properties, and to describe patterns of statistical covariance of traits that arise during the development of biological form. Armbruster and colleagues (2014) reviewed five different usages of the term integration: (1) **Statistical integration** characterizes the inference of developmental and physiological mechanisms from mere correlations. Mitteroecker (2009), Mitteroecker et al. (2012) as well as Armbruster et al. (2014) have expressed deep concerns over drawing biological conclusions from (merely statistical and not necessarily biologically meaningful) covariances of traits and therefore suggest to avoid the use of the term integration in this context. (2) **Variational integration**: Hallgrímsson et al. (2009) defined the term integration as "the tendency of a system to produce variation that is modularized and/or integrated", stressing that covariation of biological properties of an organism could be regarded as a simple variance-dependent proxy for integration or modularity. Mitteroecker et al. (2012) further clarified that, if pleiotropic factors would not vary in a sample of organisms, they would not contribute to the correlation between traits, even though they are developmentally linked. (3) **Developmental integration** is generally used to refer to the common developmental basis of biological traits through signalling cascades or, for example, growth factors that are expressed in multiple tissues, and this definition was included in the defining work on morphological integration by Olson and Miller (1958). Frequently, studies on developmental integration focus on the identification of variational modules (Wagner et al., 2007; Mitteroecker, 2009) that are interpreted as developmental modules (e.g. Klingenberg, 2008; Albertson et al., 2005).

Developmental integration ultimately also touches on the study of pleiotropic genes (genes or genetic mutations that have an effect on multiple phenotypes) as well as the genotype-phenotype map that brings about a developmental system (Lande, 1980; Pavlicev & Hansen, 2011). (4) **Functional integration**, like developmental integration, was already used by Olson and Miller (1958) and frequently serves as a basis for studies on integration. The idea behind it is that traits that serve a common functional purpose evolve and develop together in order to form a functional whole. A prominent example is the upper and lower jaw of mammals, which need to grow in a concerted way in order to enable optimal occlusion. Armbruster et al. (2014) point out that functional integration can be hard to identify, since it includes phenotypic and genetic integration, as well as other non-detectable covariation. (5) **Evolutionary integration** is defined by "the disposition for two or more traits to evolve jointly during the divergence of populations or species" (Armbruster et al., 2014, page 3). It is therefore closely related to the concept of modularity, which will be discussed below.

Given this wide spectrum of applications of the term "integration", how would one be able to detect integrated processes when analyzing biological data? Mitteroecker (2009) points out that covariation of traits should not be translated directly into claims about developmental or functional integration. For example, he states that spatial auto-correlation necessarily leads to correlations of spatially adjacent traits. In this case, statistical covariation does not necessarily originate from functional or developmental integration, a phenomenon also known as *Pearson´s rule of neighborhood* (Whiteley and Pearson, 1899, as cited in Mitteroecker et al., 2012). Furthermore, as Mitteroecker et al. (2012) wrote, variation of individual traits can overshadow patterns of covariance between them, especially if there are only minor associations. The authors also highlight the possibility that the covariances induced by two or more pleiotropic factors with opposite effects cancel, but the resulting absence of covariance does not indicate developmental or genetic independence.

Instead, the present thesis will introduce a new null-model to the study of integration. The following section will derive the null-model of self-similarity, i.e. completely irregulated growth, previously introduced by Bookstein (2015) and applied by Matiasch (2015) and Mitteroecker et al. (2019, under review). Not only does this approach take into account the covariances, as well as the individual variances, of traits, but it also presents the biologically meaningful alternative cases of coordinated or compensatory growth, in contrast to presence or absence of integrational processes, which were the consequences of previous approaches.

A toy model for the study of integration and self-similarity

In order to interpret the variance of traits in the analysis of morphological integration, consider the following toy model of two traits *A* and *B* that sum up to a total structure *S* (see also Matiasch (2015) and Mitteroecker et al. (2019, under review):

$$S = A + B \tag{1}$$

If this holds for all individuals, the average values for *A* and *B* will also add up to the average value of *S*:

$$E(S) = E(A) + E(B) \tag{2}$$

The variance of *S* in the sample is given by

$$Var(S) = Var(A + B) \tag{3}$$

And according to a well-known theorem, it can be decomposed into the variance of parts *A* and *B*, plus twice the covariance between parts *A* and *B*:

$$Var(S) = Var(A) + Var(B) + 2Cov(A, B) \tag{4}$$

This equation can be extended to decompose variation of any trait *T* consisting of parts P_i in a sample of size *n* using the following formula:

$$Var(T) = \sum_{i=1}^{n} Var(P_i) + \sum_{i \neq \mathrm{j}}^{n*(n-1)} Cov(P_i, P_j) \tag{5}$$

From the latter formula, the following modes of growth can be deduced:

1. *Coordinated growth*: The covariance of parts P_i and P_j is positive. Therefore, the overall variance of a trait *T* is larger than the summed variances of its individual parts. If one of the two sub-structures undergoes change in size, the other sub-structure will follow accordingly so that its size stays the same relative to the other one.
2. *Compensatory growth*: The covariance of parts P_i and P_j is negative. Therefore, the overall variance of a trait *S* is smaller than the summed variances of its individual sub-

structures. If one part undergoes a change in size, the other structure tends to compensate through a correlated change of size, resulting reduced of size in the overall structure.

3. *Modularity*: In this case, the covariance of parts P_i and P_j equals 0. This scenario is consistent with a complete lack of developmental integration.

The terms "coordinated growth" and "compensatory growth both reflect cases of morphological integration. Also, modularity has already been subject to extensive research (see e.g. Müller, 2007; Wagner, 1996) and has previously been defined as the near decomposability (Simon, 1962) or quasi-independence (Lewontin, 1978) of components of a biological system. The basic idea, however, dates back to Needham (1933), who introduced the term "dissociability" and coined the idea that developmental processes, while themselves highly integrated, can be separated from one another experimentally. According to Mitteroecker (2009), the main property of a biological module is its independent genetic or developmental control.

In 2015, Bookstein presented an approach to the study of integration and modularity, or self-similarity. Self-similarity is a term that generally refers to a state in which the variance of any measure relative to the spatial scale of the measurements stays the same. In the above toy model, variational self-similarity results if the covariance of these measurements is zero ("modularity"), giving rise to the following relationship:

$$V(A + B) = V(A) + V(B) \tag{6}$$

Under self-similarity, mean measure of a structure would scale linearly with its variance, irrespective of its spatial scale:

$$\frac{V(A + B)}{E(A + B)} = \frac{V(A)}{E(A)} \tag{7}$$

Plotting the variances against the means would result in a slope of 1 in a linear regression model. Any deviation from this state of self-similarity would be caused by some kind of covariation among parts. In the case of coordinated growth, variance increases more than linearly, resulting in the slope of the >1 of log variance on log mean. On the other hand, in the case of a dominance of compensatory growth processes, the variance of a structure increases less than linearly with the mean, yielding a slope <1.

It is important to note that these equations only apply to extensive measurements, such as length, area and volume measurements. Mitteroecker et al. (2019, under review) highlight that,

for measures of shape, “such analyses are limited to the non-affine aspects of landmark variation” (page 9f.). While affine shape transformations are linear transformations, such as scaling and shearing, and therefore are of infinite scale (i.e. apply to the whole landmark configuration and therefore cannot be localized), non-affine transformations can be localized and can therefore be used to investigate the degree of shape variation at different spatial scales. A measure in shape analysis capturing only non-affine shape is *bending energy*, which measures the extent of the deformation between two landmark configurations (Bookstein, 1991) and is “an inverse measure of squared spatial scale” (Mitteroecker et al., 2019, under review; page 11): Large bending energies correspond small-scale deformations, while small bending energies correspond large-scale deformations. In the following study, bending energy will be used as a shape measure analogous to mean size in the analysis of size.

Further on, shape deformations for each dimension of the landmark configuration (x- and y-coordinates in two dimensions) can be decomposed into geometrically independent components with different spatial scale, called *partial warps* (Bookstein, 1989, 1991). The corresponding partial warp scores are “the orthogonal projections of the shape vectors (as residuals from the reference shape) onto the principal warp vectors, separately for x and y” (Mitteroecker et al., 2019, under review; page 11). Principal warps are obtained by the decomposition of non-affine shape variation into geometrically independent components. In the analysis of shape, the variance of partial warp scores will be used as the equivalent of size variance in the analysis of size. For a self-similar pattern of shape variation, we expect a linear relationship between the variance of partial warp scores and inverse bending energy, i.e., a slope of 1 in the corresponding log-log plot (Bookstein, 2015, 2018).

The above presented toy model, extended by the concept of self-similarity for the study of landmark data, was previously applied to a sample of 30 human crania of diverse geographical origin by Matiasch (2015). The study found that overall cranial shape development results from an excess of compensatory growth processes, which ultimately canalize the overall shape of the human cranium. The term *canalization* was first coined by Waddington (1942), who used it to describe developmental reactions on both a genetic and an embryological level that “are adjusted so as to bring about one definite end-result regardless of minor variations in conditions during the course of the reaction” (page 563). Zelditch, Bookstein and Lundrigan (1993) wrote that canalization describes processes through which “individuals reach a common end-point despite variation in conditions encountered during ontogeny”. However, they also point out that an ontogenetic reduction in the variation of a trait can be achieved by the coordination of

reactions that lead to variation in characters (Zelditch et al., 1993). Zelditch et al. (2006) found that, provided that variation is continually arising throughout ontogeny, persistent canalization of locally disproportionately growing structures plays a key role in the establishment of patterns of integration. They state that canalization is possibly even of greater importance than coordinated growth, a finding which supports the above mentioned work by Matiasch (2015).

A novel method to studying cranial shape: global vs. local shape

Canalization of cranial shape will be investigated in an additional way. The cranium, being a composite structure of various bones, has to fulfill specific functions, such as providing a safe shell for the brain, facilitating vocalization as well as housing the masticatory apparatus. While these functions require the cranium to have a specific shape, it is in the following assumed that the extent to which these anatomical structures are realized by the different bones is, to a large extent, of lesser importance. For example, the midsagittal view of the cranial vault is largely made up of the occipital, parietal and frontal bone. The extent to which the frontal bone grows posteriorly would change the relative extent of the bone itself, but the overall shape of the cranial vault can be maintained, if there is a sufficient extent of compensatory growth in the parietal bone.

In the following, cranial shape will be represented in two different ways, namely by a global and local component:

1. *Global shape*: The outline shape of the cranium, which is presumed to represent functionally relevant aspects of cranial shape and ignores the contribution of individual bones to these functionally relevant structures. It thus captures large-scale morphological variation.
2. *Local shape*: The residual shape of the cranium after the standardization to a mean global shape. This representation of the cranium carries information on the relative contribution of individual bones to the overall structure, but lacks information on the, presumably functionally relevant, overall shape. Therefore, the local shape component largely captures small-scale variation.

Under the assumption that the functionally relevant global shape component is more constrained than the local shape component of the cranium due to the former´s higher functional relevance, canalization in the outline shape would decrease the variance of the overall shape. Canalization of cranial shape may thus be achieved by compensatory growth processes between cranial bones.

Biological background and hypotheses

Having defined the theoretical framework for this thesis, the second part of the introduction will present the biological reasoning behind the hereby presented approach to studying cranial bone development in chimpanzees and modern humans.

Over the last decades, several publications discussed the phylogenetic relationship between hominids, a group of primates which includes modern humans (*Homo sapiens*) and their closest living relatives, the great apes. The great apes include the genera *Pan* (the chimpanzee, *P. troglodytes*, as well as the bonobo, *P. paniscus*), *Gorilla* (gorillas) and *Pongo* (commonly known as orang-utans). One of the earliest genetic studies that could reliably identify *P. troglodytes*, the common chimpanzee, as the closest living relative of modern humans, was published by Ruvolo (1997), who also found that the genera *Homo* and *Pan* are more closely related to each other than either is to the genus *Gorilla*. It corroborated even earlier findings from comparisons of amino-acid sequences from the 1970s which found a close to 99% similarity of non-repetitive gene sequences between chimpanzees and modern humans (King & Wilson, 1975). Today, there is broad consensus over the phylogenetic relationships within the hominid group.

On the other hand, studies that compare hominid morphology regularly find the closest similarities between the genera *Pan* and *Gorilla*, with slight differences to the genus *Pongo*, but nearly always to the exclusion of *Homo*. For example, Mitteroecker et al. (2004) studied ontogenetic trajectories, which represent "ontogeny as a path through phenotype-time space" (Rice, 1996), among the hominid groups: The ontogenetic trajectories of African apes largely overlap, with minor differences in the onset of ontogenetic shape change, while the genus *Pongo* diverts from the common great ape trajectory, corroborating the molecular phylogeny which most often places *Pongo* as a sister group to *Pan/Homo* and *Gorilla*. However, the authors found that the ontogenetic trajectory of the genus *Homo* is clearly separated from the trajectory of its closest related sister group, *Pan*: Even at the onset of the measured ontogenetic shape change, there are considerable differences in cranial shape between the two species. Thereafter, the trajectories largely follow distinct directions. In addition, Neubauer et al. (2010) compared endocranial shape changes in *H. sapiens* and *P. troglodytes* and found non-linear ontogenetic trajectories for both species, which "indicate multiple underlying linear phases of shape changes" (Neubauer et al., 2010). They conclude that, firstly, endocranial shape is already distinct between the two species at birth, and secondly found "shared aspects of ontogenetic patterns of shape change for most of the postnatal period" (Neubauer et al., 2010, page 562).

They further state that, since postnatal shape changes are similar, especially following the eruption of the first deciduous teeth, one can assume that the last common ancestor of modern humans and chimpanzees already showed these growth patterns.

In part, the early divergence of ontogenetic trajectories between *H.sapiens* and the genus *Pan* may explained by the so-called "*neurocranial globularization*" (Lieberman et al., 2002) which occurs early in modern human ontogeny. This developmental phase is necessary to achieve the relatively large brain size of adult modern humans. At birth, chimpanzees have achieved a larger brain size relative to adult individuals compared to modern humans. Neubauer et al. (2010) state that "either this phase does not exist in chimpanzees, but it occurs prenatally, or this phase is unique to humans." (page 562).

Apart from the neurocranium, another important cranial region that has been the focus of much research is the cranial base: The cranial base largely consists of six bones: pars basilaris ossis occipitalis (the basilar part of the occipital bone, anterior to the foramen magnum), os occipital (posterior to the foramen magnum), os sphenoidale, os ethmoidale, os frontale and, on either side of the cranium, os temporale. Due to its role as the main supporting cranial structure of the brain, the cranial base has also been of particular interest to anthropologists within the scope of hominid brain evolution. In contrast to other primates, it has long been assumed that the human cranial base does not only extend during ontogeny, but in addition flexes in order to accommodate the relatively globular human brain (Lieberman et al., 2000), a process called cranial base angulation. Jeffery and Spoor (2004) termed this combined processes of flexion and extension a "retroflexion of the cranial base". However, Jeffery and Spoor (2004) suggest that the retroflexion of the cranial base is not necessarily caused by the accelerated globular growth of the human cranium, but instead is dependent on intrinsic factors of cranial base ontogeny, such as the different growth rates of cartilaginous and osseous components of the developing cranial base in perinatal and early postnatal individuals.

In addition, the development of the skull depends on the physiology of bone growth: In general, one can discriminate between desmal and chondral ossification. In the case of desmal ossification, the secretion of osteoid from connective-tissue cells is followed by the mineralization of these so-called primary ossification centers. The connective-tissue cells that produced the osteoid are soon immersed in the substrate and therefore develop into the first osteocytes. Through the inclusion of apatite, these desmal ossification centers mineralize to finally form the bone. In the case of chondral ossification, cartilage bone precursors make up the so-called primordial skeleton. White and Folkens (2005) point out that this mode of

ossification is especially important in parts of the skeleton, where rapid growth is necessary, but no strong support yet.

In the cranium, both modes of bone formation can be observed: The frontal, parietal, temporal, nasal, premaxilla, maxilla, nasal, palatine, vomer and part of the occipital bone are formed through desmal ossification, while the lower part of the occipital bone, sphenoid, and ethmoid have cartilage precursors, thus form through chondral ossification.

The aim of the hereby presented thesis is to investigate the processes involved in the development of hominid cranial form by conducting a geometric morphometric analysis of crania of different age groups of *H. sapiens* and *P. troglodytes* specimens. An application of the above presented toy model on cranial shape and size will shed light on coordinated and compensatory growth processes in the chondral and desmal regions of the cranium, while a novel approach for the distinction of global and local aspects of cranial shape development will also be presented. I aim to highlight possible differences in the realization of cranial form between the two species, and across ontogeny, as well as explain these differences with respect to bone formation and macroevolution.

Material and Methods

Sample composition

The sample consists of 83 computed tomography scans (CT-scans) as well as µCT-scans, which allow for higher resolution images compared to regular CT-scans. Slice thickness ranges from 200µm up to 500µm for regular CT-scans, and 80µm up to 120µm for µCT-scans.

The sample of *Pan troglodytes* skulls (represented by the subspecies *P. t. verus* and *P. t. troglodytes*) consists of 17 female adult, as well as a set of 27 infant (0-4 years), juvenile (5-10 years) and adolescent (10-14 years) individuals, whose sex is not considered. The ages of these specimens were determined based on their dental eruption state as described by Smith et al. (1994). Sources include the Kyoto University (access to scans via Digital Morphology Museum, KUPRI), the Museum of Comparative Zoology, Harvard University (access via morphosource.org) and the Senckenberg Naturkundemuseum, Frankfurt. An additional set of six adult and two juvenile individuals was collected from the Natural History Museum of Vienna, Austria. These skulls were scanned at the Vienna µCT-lab, University of Vienna.

The complementary sample representing *Homo sapiens* consists of 24 adult (including eight male and 16 female skulls), as well as 16 infant, juvenile and adolescent individuals, whose age

is known based on the collection record and whose sex was also not considered. The sources for these skulls include the Anatomical collection of the Medical University of Vienna, while the µCT-scans were produced at the Vienna µCT-lab, University of Vienna. In addition, two scans of skulls from adult female individuals were picked from the Terry collection managed by the National Museum of Natural History of the Smithsonian Institution, Washington, DC.

Landmark measurement

A landmark scheme consisting of 93 landmarks was developed in order to allow for homologous measurements of anatomical structures across an interspecific sample which further included multiple age stages. The scheme includes 36 anatomical ("fixed") landmarks and 57 sliding semilandmarks (for their names and definitions see **Table 1**, for their position in the cranium see **Figure 1**).

Table 1. The set of landmarks taken during data collection, including the order of measurement, names of the landmarks and definition of their position on the cranium.

Number	Landmark	Description
1	external bregma	Intersection point of Sutura sagittalis and Sutura coronalis.
2	internal bregma	Intersection point of Sutura sagittalis and sutura coronalis on the internal side of the braincase.
3	external lambda	Intersection point of Sutura sagittalis and Sutura lambdoidea.
4	internal lambda	Intersection point of Sutura sagittalis and Sutura lambdoidea on the internal side of the braincase.
5-16	*semi landmarks*	
17	optisthion	Intersection point of the posterior margin of the foramen magnum and the midsagittal plane.
18-29	semi landmarks	
30	basion	Intersection point of the anterior margin of the foramen magnum and the midsagittal plane.
31	internal posterior sphenobasillaris	Caudal intersection point of the Synchondrosis sphenooccipitalis and the midsagittal plane on the internal side of the braincase.
32	internal anterior sphenobasillaris	Rostral intersection point of the Synchondrosis sphenooccipitalis and the midsagittal plane on the internal side of the braincase.

33	“base of dorsum sellae“	Point of maximum curvature at the intersection point of the base of the dorsum sellae and the midsagittal plane.
34	“internal craniopharyngeal canal“	Point of emergence of the craniopharyngeal canal in the sella turcica.
35	“sulcus chiasmatis“	Intersection point of the caudal margin of the Sulcus chiasmatis and the midsagittal plane.
36	“jugum sphenoidale“	Intersection point of the jugum sphenoidale and the midsagittal plane.
37	*semi landmark*	
38	hormion	Projection of the most caudal points of the alae vomeris onto the midsagittal plane.
39	“external posterior basioccipital“	Caudal intersection point of the Synchondrosis sphenooccipitalis and the midsagittal plane on the external side of the braincase.
40	“external anterior postsphenoid“	Rostral intersection point of the Synchondrosis sphenooccipitalis and the midsagittal plane on the internal side of the braincase.
41	“external craniopharyngeal canal“	Point of emergence of the craniopharyngeal canal on the internal side of the cranial base.
42	vomer	The most superior point of contact of vomer and os sphenoidale.
43	*semi landmark [vomer]*	
44	*semi landmark [sphenoid]*	
45	*semi landmark [ethmoid]*	
46	spina ethmoidalis	Tip of the spina ethmoidalis, caudal margin of the gap between os ethmoidale and os sphenoidale.
47	posterior cribriform plate	Most caudal intersection point of the lamina cribrosa and the midsagittal plane.
48	*semi landmark*	
49	anterior cribriform plate	Most rostral intersection point of the lamina cribrosa and the midsagittal plane (not necessarily at the foramen caecum).
50	projection of ant. cribr. plate	
51	anterior perpendicular plate	Most anterior point of lamina perpendicularis in contact with os nasale/os frontale.

52	akanthion	Most inferior point of apertura piriformis.
53	anterior vomer	Most rostral point of the vomer.
54	*semi landmark*	
55	*semi landmark*	
56	prosthion	Most rostral point of the alveolar ridge in the midsagittal plane.
57	orale	Orthogonal projection of the prosthion onto the inner side of the alveolar ridge.
58	posterior nasal spine	Rostral point of the spina nasalis close to the midsagittal plane.
59	palato-vomerale	Most posterior point of contact between os palatinum and vomer.
60	*semi landmark*	
61	superior incisive canal	Superior point of emergene of canalis incisivus.
62	inferior incisive canal	Inferior point of emergence of canalis incisivus.
63-66	*semi landmark*	
67	superior palatomaxillare	Superior intersection point of Sutura palatina mediana and Sutura palatina transversa.
68	inferior palatomaxillare	Inferior intersection point of Sutura palatina mediana and Sutura palatina transversa.
69 & 70	*semi landmarks*	
71	rhinion	Most anterior point of Sutura internasalis.
72	nasion	Most superior point of Sutura internasalis.
73	*semi landmark*	
74 & 75	*semi landmarks*	
76	fronto-nasale	Most inferior point of Sutura nasofrontalis.
77	semi landmark	
78	glabella	Most anterior midsagittal point of os frontale.
79-90	*semi landmarks*	
91	*semi landmark [ethmoid]*	
92	*semi landmark [frontal]*	
93	*semi landmark [ethmoid]*	

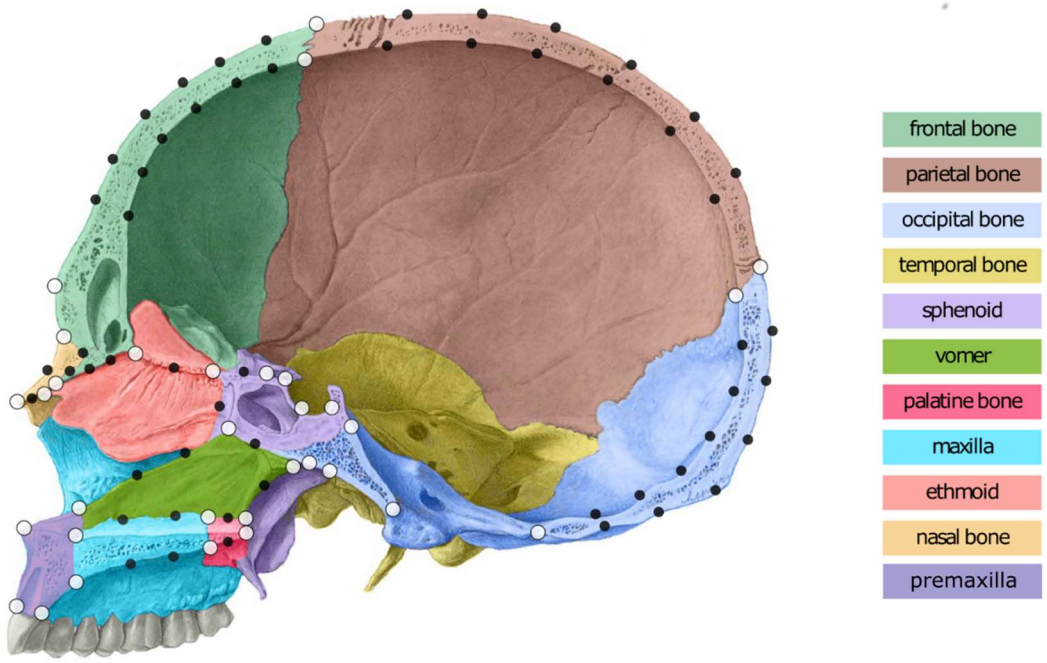

Figure 1. Midsagittal view of the human cranium showing the landmark set that is used in this thesis. White dots indicate anatomical landmarks, black dots indicate semilandmarks and orange dots indicate paired landmarks on either side of sutures between bones that close during ontogeny.

In contrast to predefined, "real" landmarks that can be placed at an anatomical point location, such as the intersection of two sutures, Mitteroecker et al. (2013) described semilandmarks as "points on smooth curves, for which the exact location on the curve cannot be identified and hence is statistically estimated." Following this definition, the semilandmarks defined in the present scheme delineate regions such as the external and internal skullcap or the fronto-nasal suture (see **Figure 2** for an illustration of semilandmarks and their respective tangents). All landmarks are located in the midsagittal plane of the skull and their positions are chosen in order to delineate the midsagittal outline of the following cranial bones: frontal bone, parietal bone, occipital bone (including pars basilaris), sphenoid, ethmoid, vomer, premaxilla, maxilla, palatine bone and the nasal bone. **Table 2** gives a list of the different cranial components and their delineating landmarks.

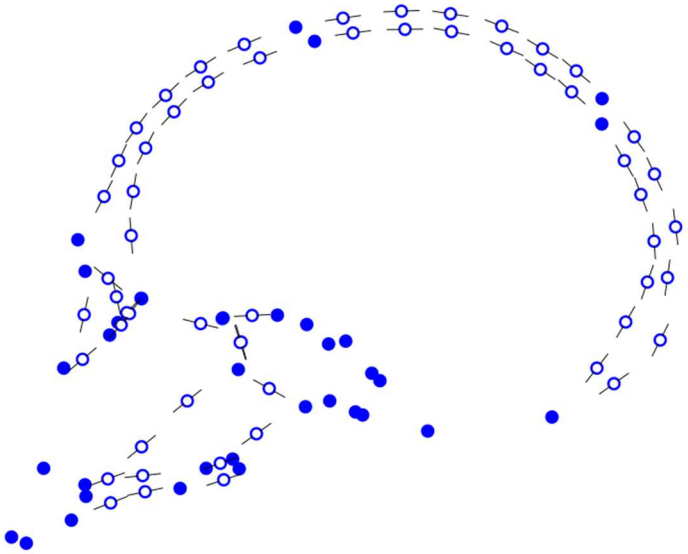

Figure 2. The set of landmarks measured on a non-adult chimpanzee. Filled dots indicate anatomical landmarks (N = 37), empty dots indicate semilandmarks (N = 57) and their associated sliding tangents

Table 2. Bone definitions for the overall cranium.

Bone	Delineating landmarks
frontal bone	1,89,87,85,83,81,79,78,72,74,75,76,92,50,80,82,84,86,88,90,2
parietal bone	1,5,7,9,11,13,15,3,4,16,14,12,10,8,6,2
occipital bone	3,18,20,22,24,26,28,17,29,27,25,23,21,19,4
occipital bone (pars basilaris)	30,31,39
sphenoid	32,33,34,35,36,37,46,44,42,43,38,41,40
ethmoid	47,48,49,91,93,51,42,45
vomer	53,54,55,42,43,38,60,59,69,67,65,63,61
praemaxilla	52,56,57,62,61,53
maxilla	61,63,65,67,68,66,64,62
palatine bone	67,69,59,58,70,68
nasal bone	72,73,71,77,76,75,74

The placement of landmarks was performed using the Amira software package (version 6.4.0) which was installed on an Apple MacPro machine running macOS Sierra (version 10.12.6). All CT-images as well as µCT-data were loaded into the software in TIFF, DICOM or UNIX executable format. Landmarks were measured in a locally defined midsagittal plane in order to account for natural irregularities of cranial bone growth and to represent each structure as precise as possible. The 3D visualizations of the crania were mainly achieved using orthogonal

slices, volume renderings, as well as isosurfaces. Placement of semi-landmarks along the curvature of the skull cap was based on manually selected sections through the image stack.

Landmark pre-processing

Preprocessing of landmark coordinates was conducted using the R software (version 3.5.1) via the interface Rstudio (version 1.1.463). To ensure that the order of landmarks was the same across all specimens (a crucial prerequisite for the statistical analysis of landmark data) the following steps were undertaken for each species and age group separately. A so-called generalized Procrustes analysis (below referred to as "GPA") was performed to ensure that the landmark data merely differed by the relative positions of landmarks. The aim of the GPA is to facilitate the analysis of shape of a measured object irrespective of its location, size or orientation. This three-step algorithm is based on the Procrustes superimposition as described by Gower (1975) that was later extended by Rohlf and Slice (1990). In the first step, it translates all landmark configurations to the same centroid (the mean coordinates for all landmarks in an object), which eliminates information on the location of all objects. In order to standardize for the size of the objects, their landmark configurations are scaled to have the same *Centroid Size*, a measure calculated by "the square root of the summed squared deviations of the coordinates from their centroid" (Mitteroecker & Gunz, 2009). In the last step, the objects are rotated based on a least-squares approach, meaning that the sum of the squared distances between homologous landmarks is minimized.

Following the GPA, a principal component analysis (PCA) was used to reveal misplaced landmarks. Where necessary, disarranged landmarks were corrected in Amira. For an additional visual control of the correct placement of landmarks, the connecting lines between neighbouring landmarks were plotted for each skull to delineate each bone separately. Where necessary, the raw landmark file was corrected.

As mentioned above, the midsagittal plane was assessed locally and needed to be redefined regularly to account for natural irregularities of cranial bone growth. Before further analysis, the raw 3D coordinates were projected on a single 2D plane, representing the common midsagittal plane, for each specimen separately. In order to retain the between-individual variation of interest, all landmarks were projected into a coordinate system spanned by the first and second principal component of the landmark coordinates of the respective specimen. From this point of the analysis onwards, the first and second principal component scores of each

landmark were treated as the X and Y coordinates in the newly defined two-dimensional coordinate space.

The geometric morphometric analysis of the data was largely conducted using the R-packages "geomorph" (version 3.0.7) and "Morpho" (version 2.6). Other code that was written can be found in the appendix of this thesis, together with the landmark definitions of the outine shape, the chondrocranial and desmocranial outline, as well as the individual bones.

Analysis of size

For the analysis of size and shape of the cranium, each bone, as well as the overall shape of the cranium and its components, the chondrocranium and the desmocranium (see chapter "Biological background and hypotheses"), was delineated by a subset of two-dimensional landmarks. Following the reasoning of the above presented toy model, the size variance of each individual bone, as well as the overall structure, was calculated (see Appendix for R code).

Further on, a test for self-similarity was conducted. To this end, the natural logarithm of the variance of the size of each bone that contributes to the size of the overall cranium, was plotted against the natural logarithm of the mean size of these bones. The same procedure was followed for the chondrocranium and desmocranium separately. A linear model was fitted to calculate the slopes of these regressions

Analysis of shape

To investigate the growth processes of the shape of the cranium, the overall shapes of the cranium, as well as the contributing bones, were first subjected to separate Procrustes superimpositions in each of the four sample groups (i.e. species and age groups). Subsequently, the sum of the variance for the x and y coordinates of each structure represented the total shape variance of the latter. In order to take into account the number of landmarks of the structures, one has to divide the variance of each landmark configuration (delineating each bone) by the number of landmarks. Accordingly, one has to adjust the centroid size, which is the square root of the sum of squared distances of the landmark to the centroid (and therefore likewise dependent on the number of landmarks in a structure), by multiplying the Procrustes coordinates by the square root of the number of landmarks. In the end, these two operations cancel, which means that one can directly compare the shape variances of the individual bones without any further standardization for the number of landmarks (Mitteroecker et al., 2019; under review).

To test for self-similarity, a measure analogous to mean bone size and bone size variance in the previous analysis had to be used: The bending energy, which is the extent of the non-affine bending of the deformation grid when comparing two sets of landmarks, can be used as a measure of scale, analogous to mean bone size. Since large bending energies are indicative of localized shape changes, and vice versa, the inverse bending energy was used for better and more intuitive visualization. The variances of the partial warps of both the x and the y coordinates of each landmark were used as a measure of variance. The natural logarithms of the variances of the partial warps were plotted against the natural logarithms of the inverse bending energies. Again, a linear regression model was calculated to obtain the values for the slopes (Bookstein, 2015; Mitteroecker et al., 2019; under review; see Appendix for R code).

Global and local components of cranial shape

For the discrimination between overall shape, representing the functionally relevant aspects of cranial shape, and residual shape, which retains information on the contribution of individual bones to structures of the hominid cranium, the full landmark set, consisting of 36 fixed landmarks and 57 sliding semilandmarks, was split into two sets of landmarks: The first set comprised 60 landmarks, which together form the outline shape. It therefore includes the cranial vault and the cranial base, which together form the braincase, as well as the outline shape of the viscerocranium, capturing, e.g., facial prognathism, a key feature which separates human from great ape morphology. In order to construct a mean global shape across all individuals of the sample, only twelve type 2 landmarks (p=12), the extreme points of the cranial base, the viscerocranium and the foramen magnum, were treated as fixed landmarks. Type 1 landmarks, which were originally placed at points of intersection between bones, were treated as semilandmarks in order to eliminate information on the relative extents of the bones in the cranium.

The second set of landmarks includes all 93 landmarks and represents the local shape component of the cranium. It is obtained by warping the landmark set to the mean outline shape (see **Figure 3**) calculated based on the previous set using the "thin plate spline" algorithm, which minimizes bending energy between homologous landmark configurations (Bookstein, 1989). For this procedure, only those landmarks that were originally defined as semilandmarks were allowed to slide along their respective tangents, and type 1 landmarks are once again treated as anatomical landmarks.

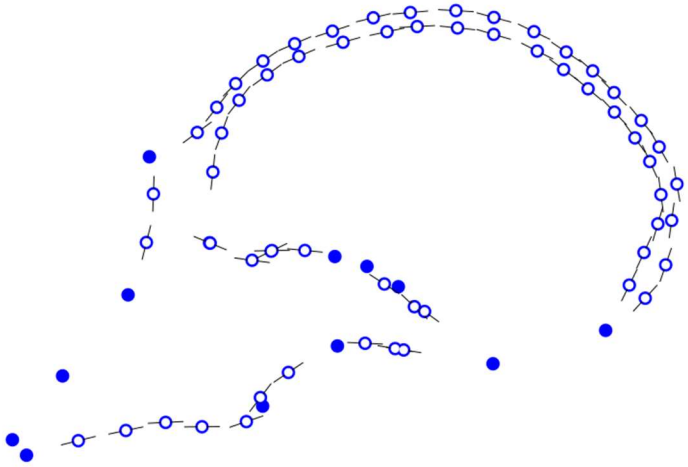

Figure 3. Mean outline shape including semilandmarks (p = 48) and their associated tangents (empty points) and type 2 anatomical landmarks (p = 12, filled points) that were treated as fixed landmarks.

Results

Size analysis

Overall cranium

Figure 4 clearly shows that overall size is much more variable than the sum of the variances of the individual bones within all sample groups. In adult humans, for example, the overall variance was 495,212mm^2, while the sum of the variances of individual bones was 115,512mm^2. This same pattern can be observed in the non-adult human and both chimpanzee samples (variances are reported in **Table 3**).

Table 3. Results of the unstandardized size variance analysis for the overall cranium. Note the difference between the sum of the variances of the individual bones and the variance calculated for the overall cranium directly ("overall").

	variance (mm^2)			
bone	*adult human*	*non-adult human*	*adult chimpanzee*	*non-adult chimpanzee*
parietal	15,144.96	12,465.43	3,602.26	5,982.80
occipital	26,856.98	13,095.22	4,975.15	5,364.01
basioccipital	1,190.49	778.78	1,217.51	1,379.06
sphenoid	6,931.19	7,182.11	4,848.02	16,769.99
vomer	14,897.62	13,727.46	10,897.44	27,636.36
ethmoid	10,907.95	14,297.67	4,826.04	12,781.61
premaxilla	2,452.33	1,411.62	2,230.67	6,509.11
maxilla	1,394.31	1,417.57	2,238.63	5,775.67
palatine	588.82	284.48	661.53	736.32
nasal	633.92	356.82	1,927.81	3,925.45
frontal	34,513.89	29,918.40	13,536.40	40,792.30
sum of bones	115,512.5	94,935.56	50,961.47	127,652.7
overall cranium	495,212.55	775,715.44	194,414.06	1,363,191.71

Figure 5 shows that, after standardization of the variances by the mean, the size variance of the overall cranium is generally higher in the non-adult than in the adult groups, with adult chimpanzees being the least variable and non-adult chimpanzees the most variable in terms of size of the overall cranium. Mean-standardized variances for the individual bones as well as for the total cranium for humans and chimpanzees, by age group, are listed in **Table 4**. Generally,

the size of the cranium and its components is more variable in the non-adult samples compared to the adult samples, except for some modern human bones (see **Table 4**).

Lastly, **Figure 6** gives the linear regression models for each sample group. The slopes range from a maximum of 1.77 in the non-adult chimpanzee sample to a minimum of 1.33 for adult chimpanzees, all of which are substantially higher than 1, indicating a faster than linear increase of variance with average size in all groups.

Table 4. Detailed results for the standardized variance analysis of all sample groups.

	variance/mean (mm)			
bone	*adult human*	*non-adult human*	*adult chimpanzee*	*non-adult chimpanzee*
parietal	22.87	36.92	14.04	26.23
occipital	33.98	28.04	16.47	22.16
basioccipital	9.87	7.79	10.23	16.49
sphenoid	12.15	17.21	8.71	43.69
vomer	23.14	30.22	18.07	64.67
ethmoid	20.43	54.59	12.69	66.50
premaxilla	10.66	9.16	7.42	31.94
maxilla	8.38	16.86	12.70	42.29
palatine	7.92	7.14	10.55	16.02
nasal	7.73	7.94	11.20	27.26
frontal	37.30	55.78	18.63	85.14
overall	85.22	213.48	43.53	418.82

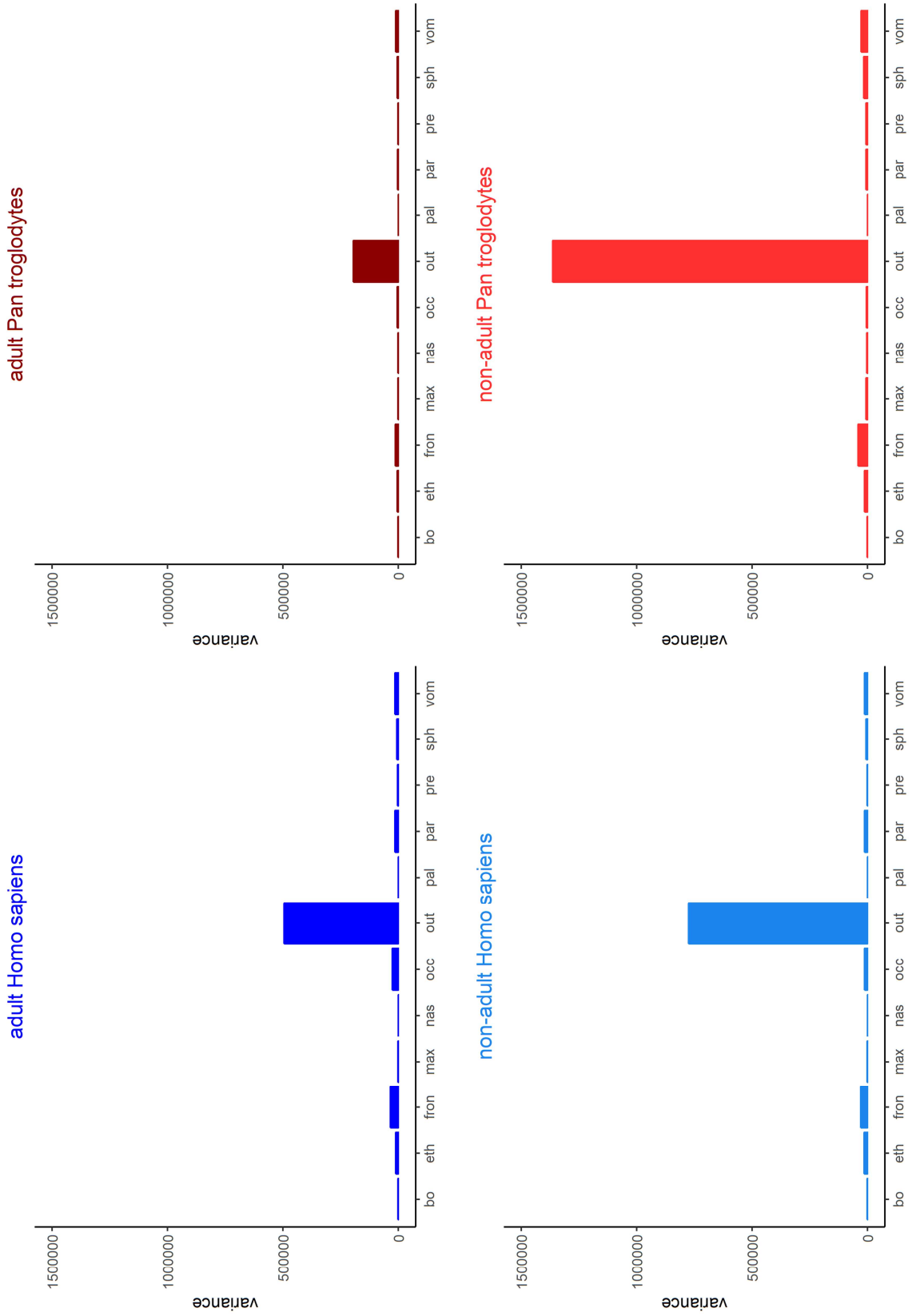

Figure 4. Barplots for size variance analysis of the overall cranium. The variance of the overall cranium is consistently higher than the sums of the variances of the individual bones. (bo=basioccipital, eth=ethmoid, fron=frontal bone, max=maxilla, nas=nasal bone, occ=occipital bone, out=outline, pal=palatine bone, par=parietal bone, pre=premaxilla, sph=sphenoid, vom=vomer)

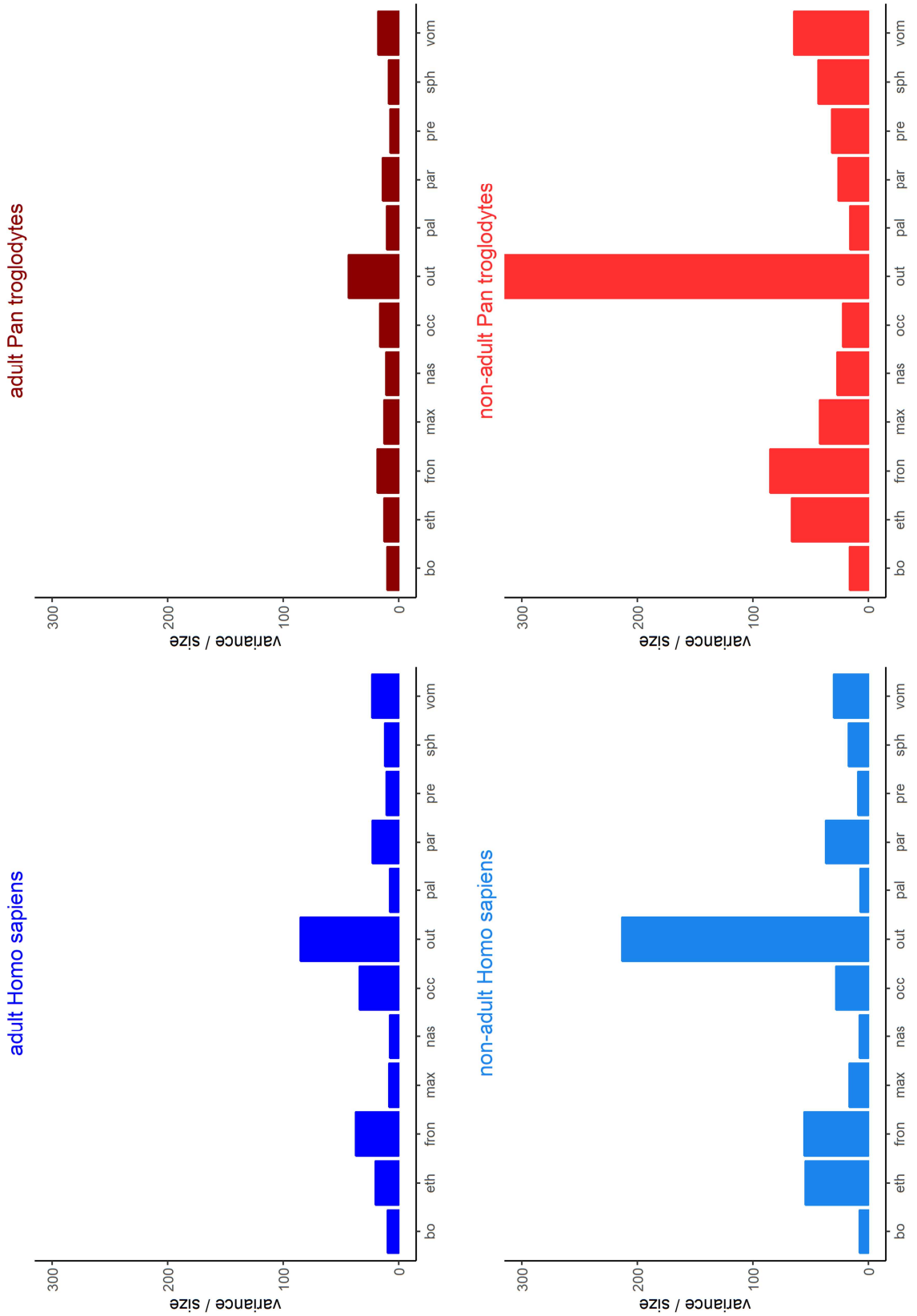

Figure 5. Barplots for size analysis of the standardized variances. Generally, the non-adult groups are considerably more variable than adult groups. (bo=basioccipital, eth=ethmoid, fron=frontal bone, max=maxilla, nas=nasal bone, occ=occipital bone, out=overall, pal=palatine bone, par=parietal bone, pre=premaxilla, sph=sphenoid, vom=vomer)

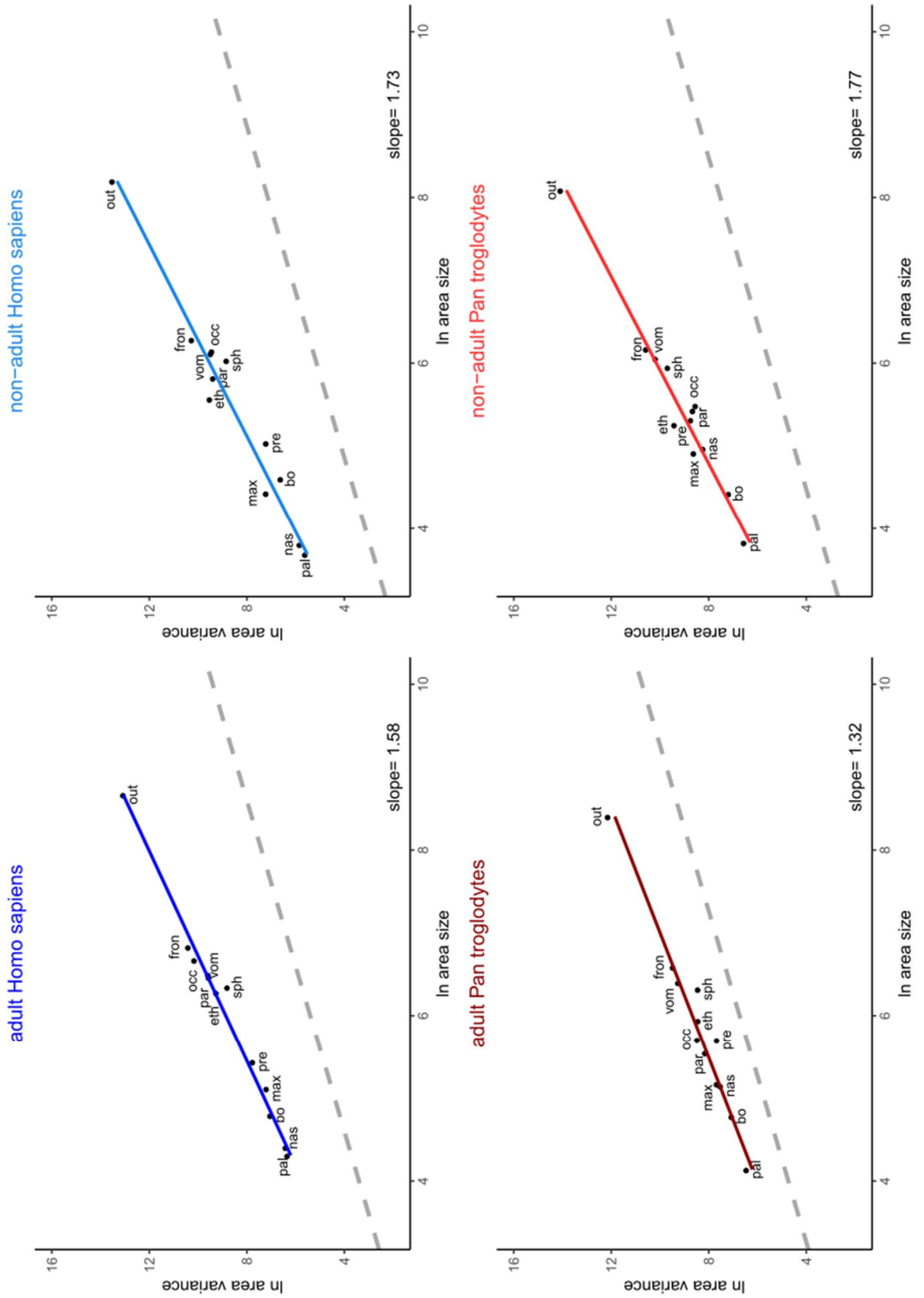

Figure 6. Scatter plots of the regression of log-transformed size variance onto log-transformed mean size. The grey dotted line indicates a reference regression line with slope=1 and the same intercept as the respective regression model. (bo=basioccipital, eth=ethmoid, fron=frontal bone, max=maxilla, nas=nasal bone, occ=occipital bone, out=outline, pal=palatine bone, par=parietal bone, pre=premaxilla, sph=sphenoid, vom=vomer)

Chondrocranium

Across all sample groups, except for the adult chimpanzees, the sum of the variance of the individual bones does not exceed the variance of the overall chondrocranium (**Table 5**, **Figure 7**). Once standardized by the mean, the variance in cranial size is overall higher in the non-adult than in the adult samples (see **Table 6**). The size variation of the sphenoid and ethmoid for non-adult chimpanzees is particularly high. Likewise, the ethmoid of non-adult humans appears to be very variable for its size (see also **Figure 8**).

Furthermore, **Figure 9** shows that, also in the chondrocranium, the variance in cranial sizes increases faster than linearly with mean size (all slopes are >1), except in adult chimpanzees (slope=0.96). Regression slopes are highest in the non-adult sample groups.

Table 5. Detailed results for size analysis of the chondrocranium for all sample groups. In all groups, except for adult chimpanzees, the variance of the overall chondrocranium is larger than the summed variances of the individual bones.

	variance (mm^2)			
bone	*adult human*	*non-adult human*	*adult chimpanzee*	*non-adult chimpanzee*
occipital	26,856.98	13,095.22	4,975.15	5,364.01
basioccipital	1,190.49	778.78	1,217.51	1,379.06
sphenoid	6,931.19	7,182.11	4,848.02	16,769.99
ethmoid	10,907.95	14,297.67	4,826.04	12,781.61
sum of bones	45,886.61	35,353.78	15,866.72	36,294.67
overall	72,048.81	77,803.78	13,861.98	85,143.60

Table 6. Detailed results for the analysis of the standardized variances for the chondrocranium.

	variance/mean (mm)			
bone	*adult human*	*non-adult human*	*adult chimpanzee*	*non-adult chimpanzee*
occipital	33.98	28.04	16.47	22.16
basioccipital	9.87	7.79	10.23	16.49
sphenoid	12.15	17.21	8.71	43.69
ethmoid	20.43	54.59	12.69	66.50
overall	39.54	66.27	10.85	100.29

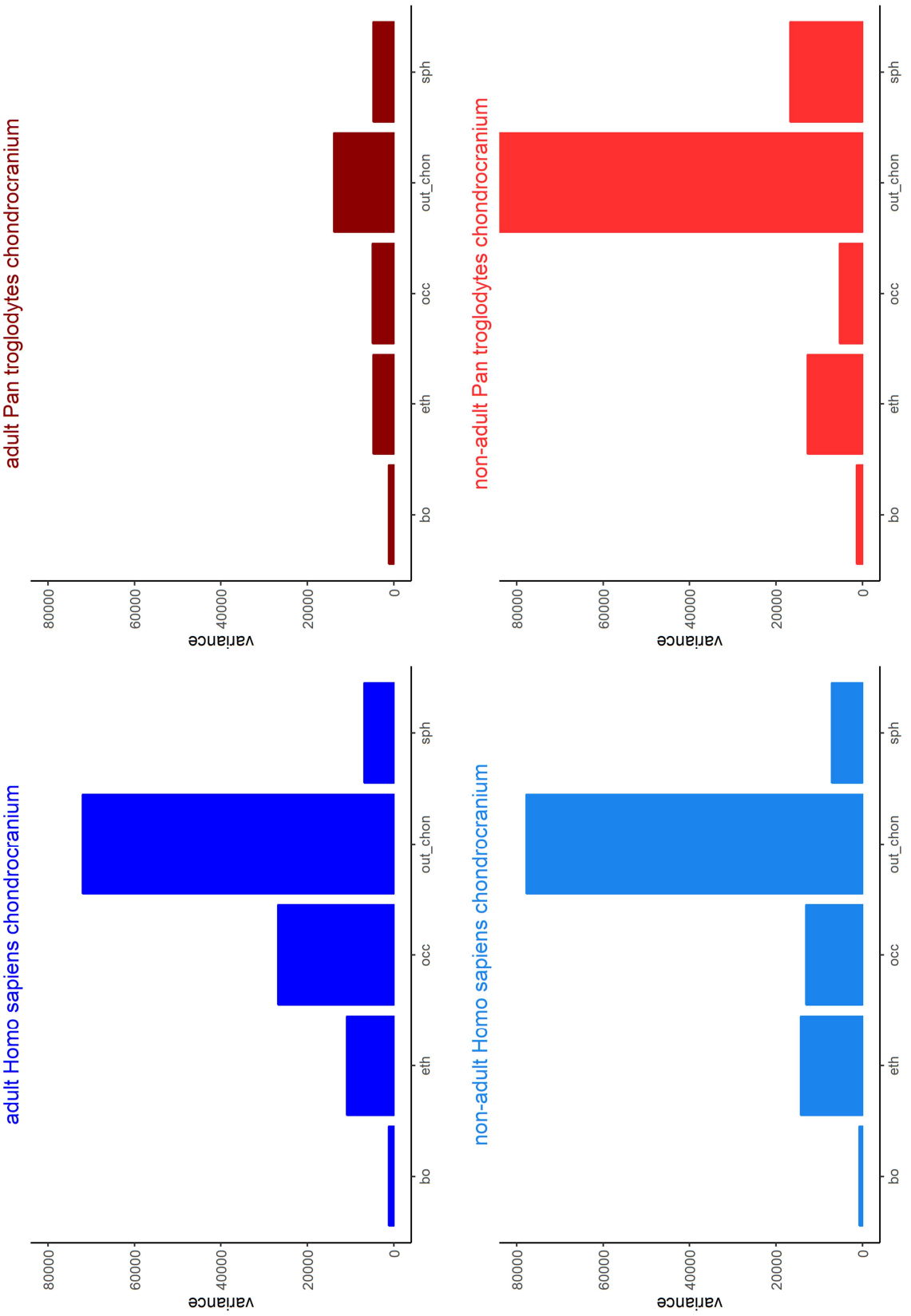

Figure 7. Barplots for the analysis of unstandardized size variance of the chondrocranium for all sample groups. (bo=basioccipital, eth=ethmoid, occ=occipital bone, out=overall, sph=sphenoid)

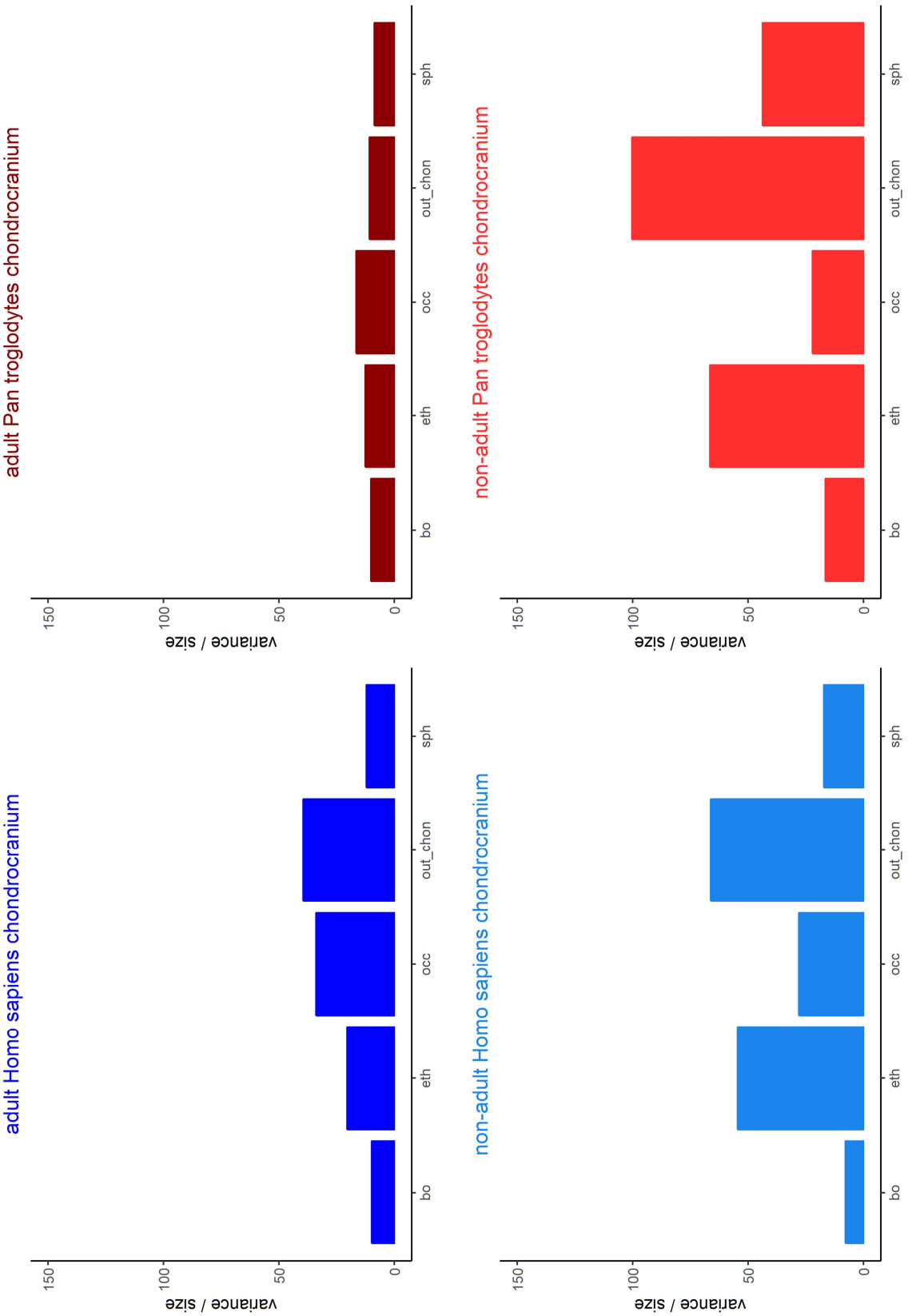

Figure 8. Barplots for the results the analysis of size variance standardized by mean size. (bo=basioccipital, eth=ethmoid, occ=occipital bone, out=overall, sph=sphenoid)

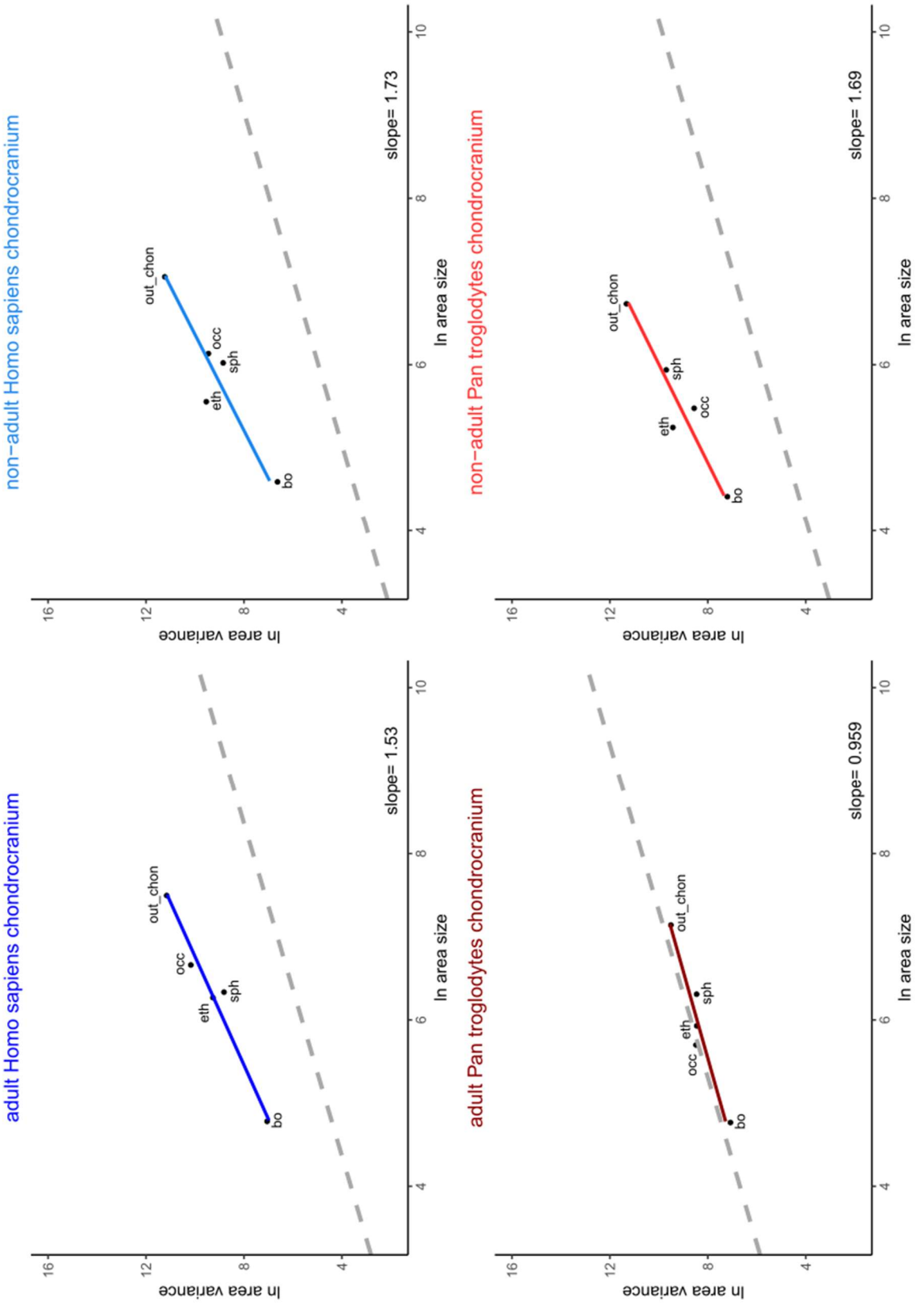

Figure 9. Scatter plots for the regression of log-transformed size variance on log-transformed mean size for the chondrocranium. The grey dotted line indicates a reference regression line with slope=1 and the same intercept as the respective regression model. Except for adult chimpanzees, variance increases faster than linearly in all groups. (bo=basioccipital, eth=ethmoid, occ=occipital bone, out_chon=chondrocranium, sph=sphenoid)

Desmocranium

Table 7 and **Figure 10** show similar results for the desmocranium: total desmocranial size has a higher variance than the sum of the individual dermal bones. Desmocranial size is relatively more variable in non-adults than adults (see **Table 8** and **Figure 11**). Besides the frontal bone, which is highly variable in all groups both in absolute terms and relative to its mean size, the size of the vomer is also highly variable in the non-adult chimpanzee sample. **Figure 12** illustrates that, once again, the regression slopes of log variance on log size are >1 in all sample groups, with the non-adult age groups having the steepest slope.

Table 7. Detailed results of the analysis of size variance in the desmocranium.

	variance (mm^2)			
bone	*adult human*	*non-adult human*	*adult chimpanzee*	*non-adult chimpanzee*
parietal	15,144.96	12,465.43	3,602.26	5,982.80
vomer	14,897.62	13,727.46	10,897.44	27,636.36
premaxilla	2,452.33	1,411.62	2,230.67	6,509.11
maxilla	1,394.31	1,417.57	2,238.63	5,775.67
palatine	588.89	284.48	661.53	736.32
nasal	633.92	356.82	1,927.81	3,925.45
frontal	34,513.89	29,918.40	13,536.40	40,792.30
sum of bones	69,625.92	59,581.78	35,094.75	91,358.03
outline	131,189.51	222,000.87	61,070.34	425,009.98

Table 8. Detailed results of the analysis of size variance standardized against mean size in the desmocranium.

	variance/mean (mm)			
bone	*adult human*	*non-adult human*	*adult chimpanzee*	*non-adult chimpanzee*
parietal	22.87	36.92	14.04	26.23
vomer	23.14	30.22	18.07	64.67
premaxilla	10.66	9.16	7.42	31.94
maxilla	8.38	16.86	12.70	42.29
palatine	7.92	7.14	10.55	16.02
nasal	7.73	7.94	11.20	27.26
frontal	37.30	55.78	18.63	85.14
outline	45.48	129.42	26.10	249.36

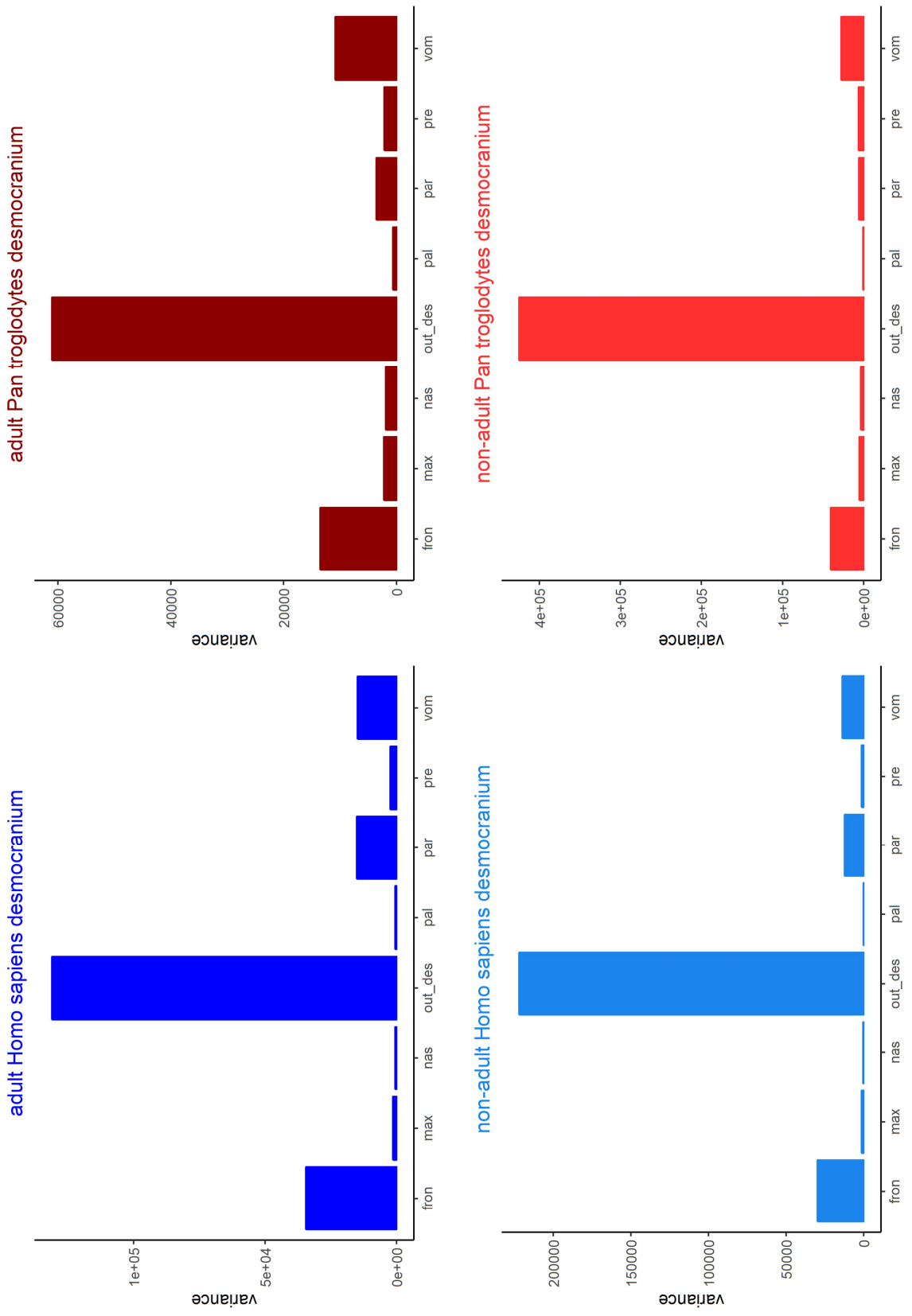

Figure 10. Barplots for size variance analysis of the desmocranium for all groups. (fron=frontal bone, max=maxilla, nas=nasal bone, out_des=desmocranium, pal=palatine bone, par=parietal bone, pre=premaxilla, vom=vomer)

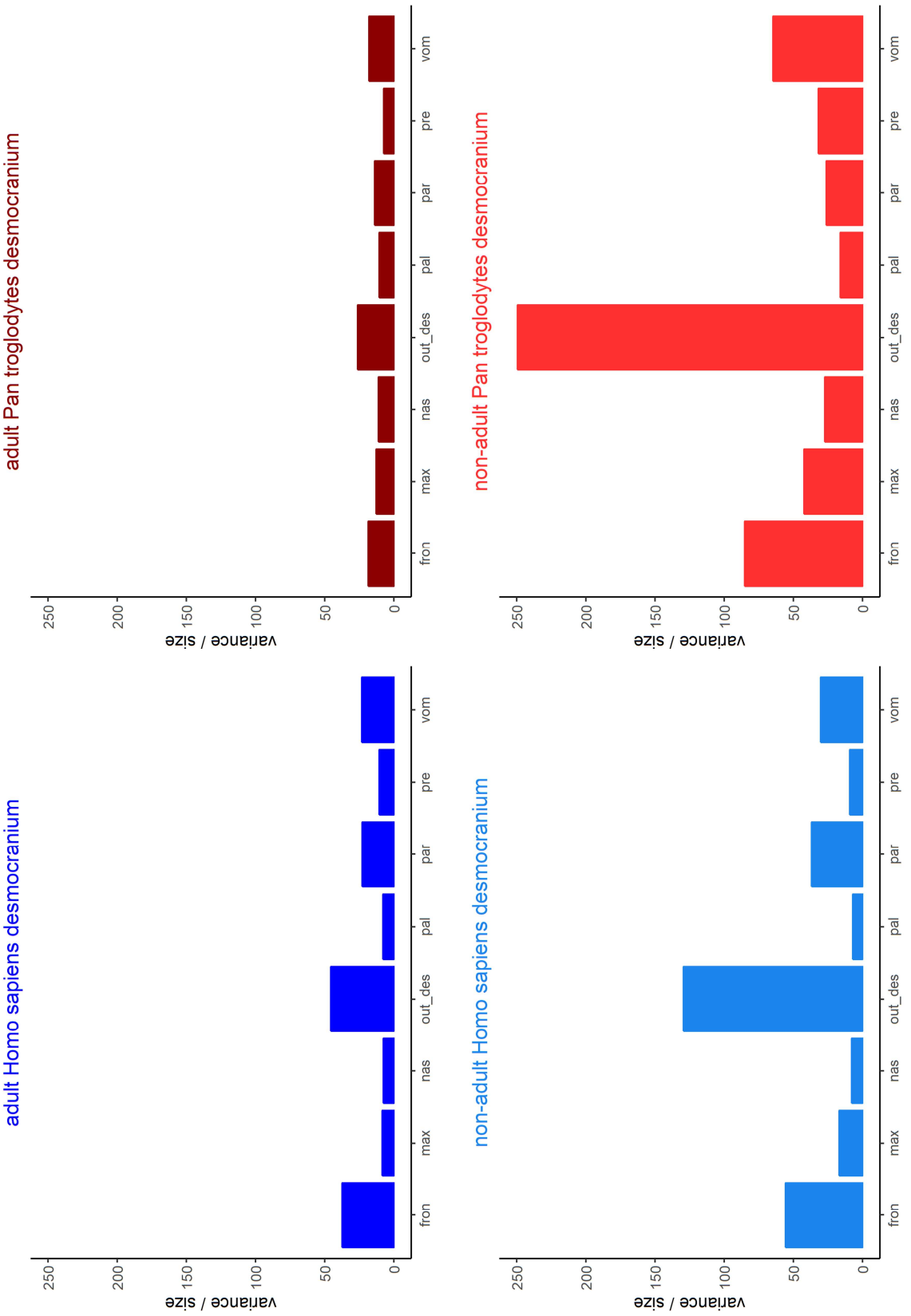

Figure 11. Barplots for the analysis of size variance standardized against mean size for all sample groups. (fron=frontal bone, max=maxilla, nas=nasal bone, out_des=desmocranium, pal=palatine bone, par=parietal bone, pre=premaxilla, vom=vomer)

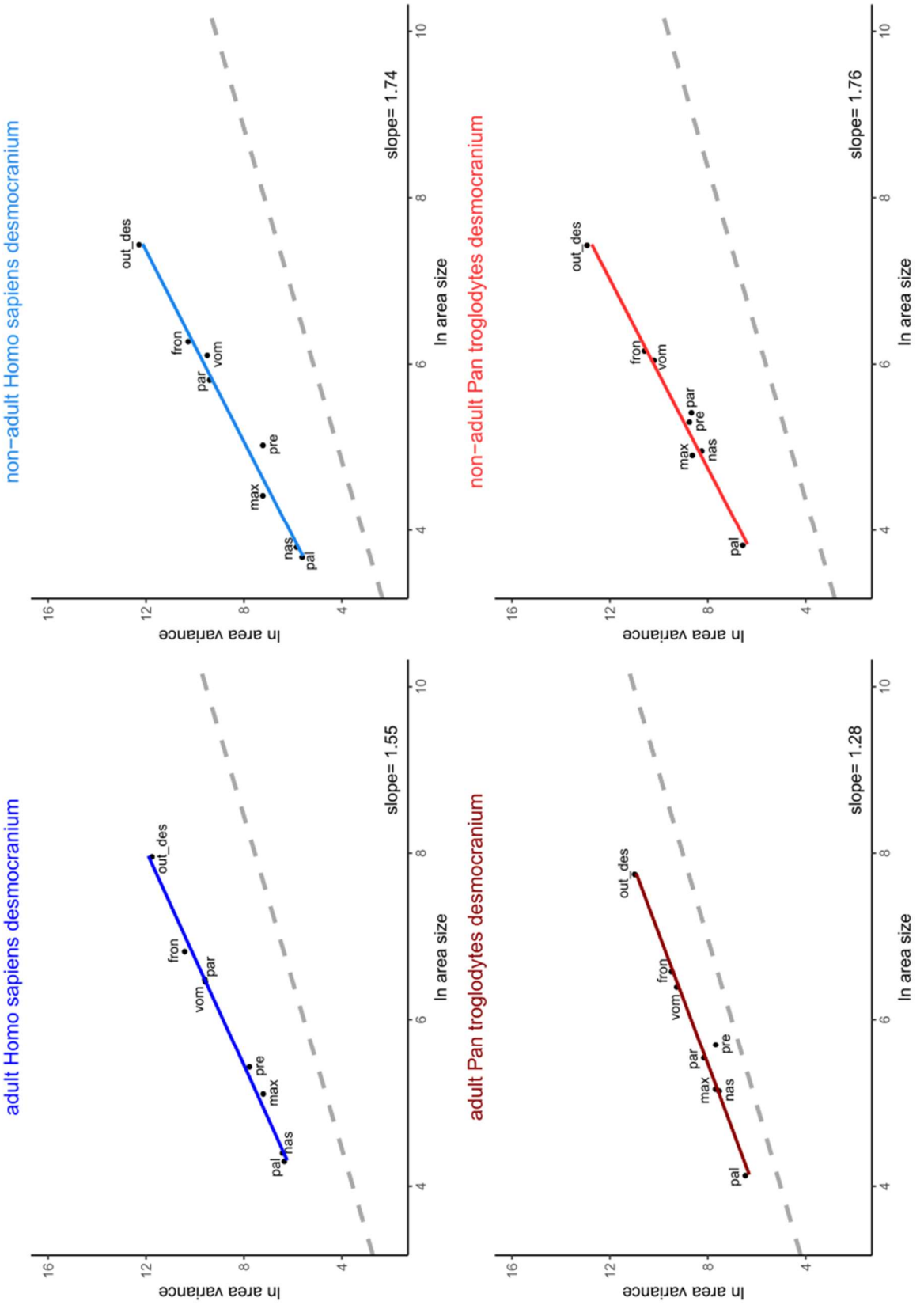

Figure 12. Scatter plots for the linear regression models of log-transformed size variances onto log-transformed mean sizes. The grey dotted line indicates a reference regression line with slope=1 and the same intercept as the respective regression model. (fron=frontal bone, max=maxilla, nas=nasal bone, out_des=desmocranium, pal=palatine bone, par=parietal bone, pre=premaxilla, vom=vomer)

Analysis of shape

Overall

In contrast to size, the shape variances of the individual bones are high compared to the shape variance of the overall cranium for all sample groups. Also, **Table 9** and **Figure 13** show that smaller bones, such as the palatine bone or the nasal bone, have higher variances compared to larger bones, such as the frontal or the parietal bone.

The linear regression models of the log-transformed partial warps onto the log-transformed inverse bending energy (see **Figure 14**) give slopes <1 for all sample groups. Note that the slopes for the non-adult samples are lower than those of the adult groups.

Table 9. Detailed results for shape variance analysis of all groups. The summed variances of each bone are larger than the variance of the overall cranium for all sample groups.

	shape variance			
bone	*adult human*	*non-adult human*	*adult chimpanzee*	*non-adult chimpanzee*
parietal	0.0017	0.0008	0.0021	0.0029
occipital	0.0048	0.0028	0.0063	0.0062
basioccipital	0.0143	0.0036	0.0100	0.0038
sphenoid	0.0209	0.0384	0.0203	0.0239
vomer	0.0216	0.0164	0.0162	0.0145
ethmoid	0.0220	0.0639	0.0176	0.1008
premaxilla	0.0396	0.0377	0.0122	0.0206
maxilla	0.0302	0.0292	0.0250	0.0240
palatine	0.0668	0.0321	0.0426	0.0614
nasal	0.0428	0.0495	0.0221	0.0418
frontal	0.0034	0.0025	0.0044	0.0117
sum of variances	0.2682	0.2768	0.1789	0.3114
overall	0.0022	0.0020	0.0032	0.0066

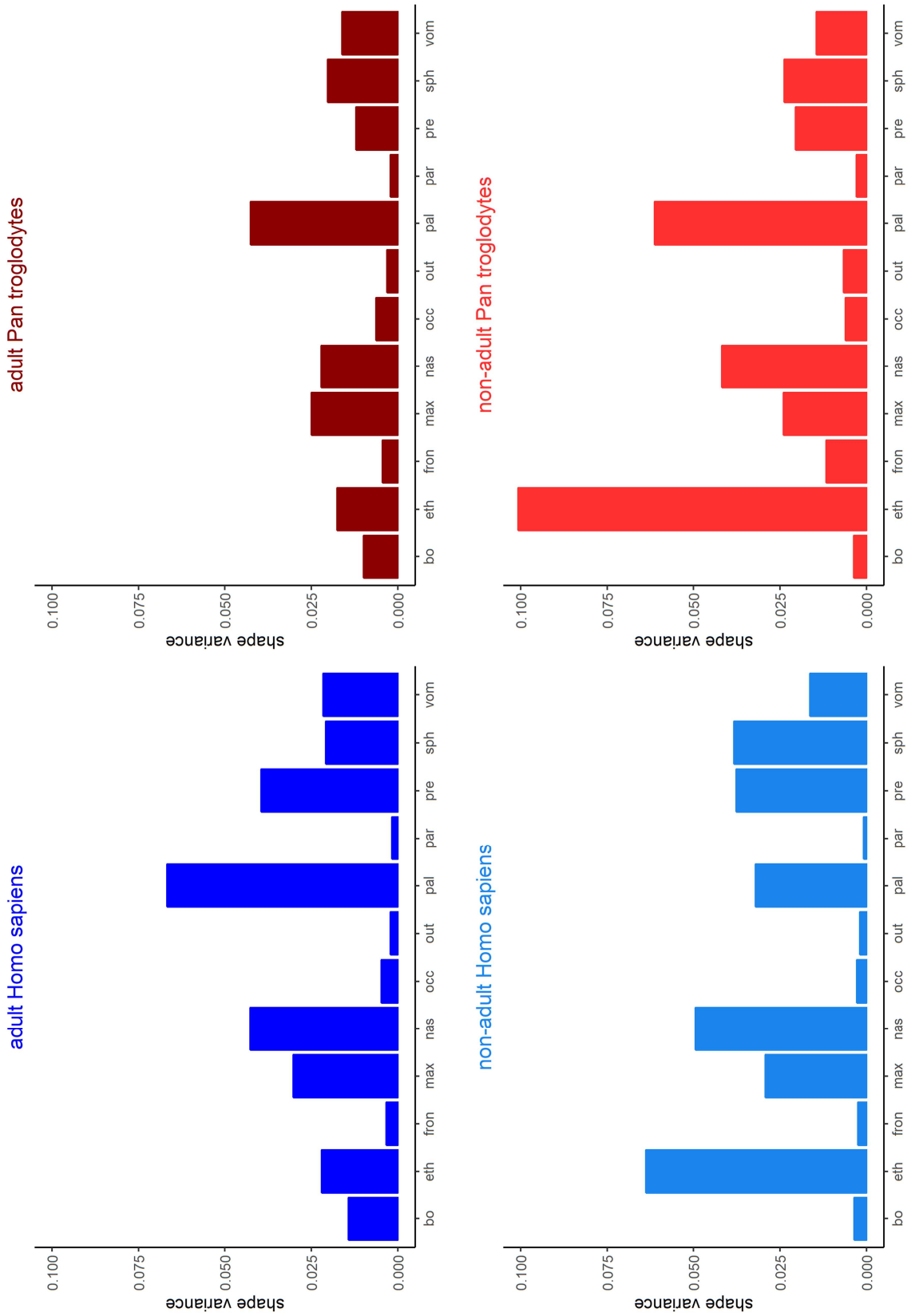

Figure 13. Barplots for shape variance analysis of the overall cranium. (bo=basioccipital, eth=ethmoid, fron=frontal bone, max=maxilla, nas=nasal bone, occ=occipital bone, out=overall, pal=palatine bone, par=parietal bone, pre=premaxilla, sph=sphenoid, vom=vomer)

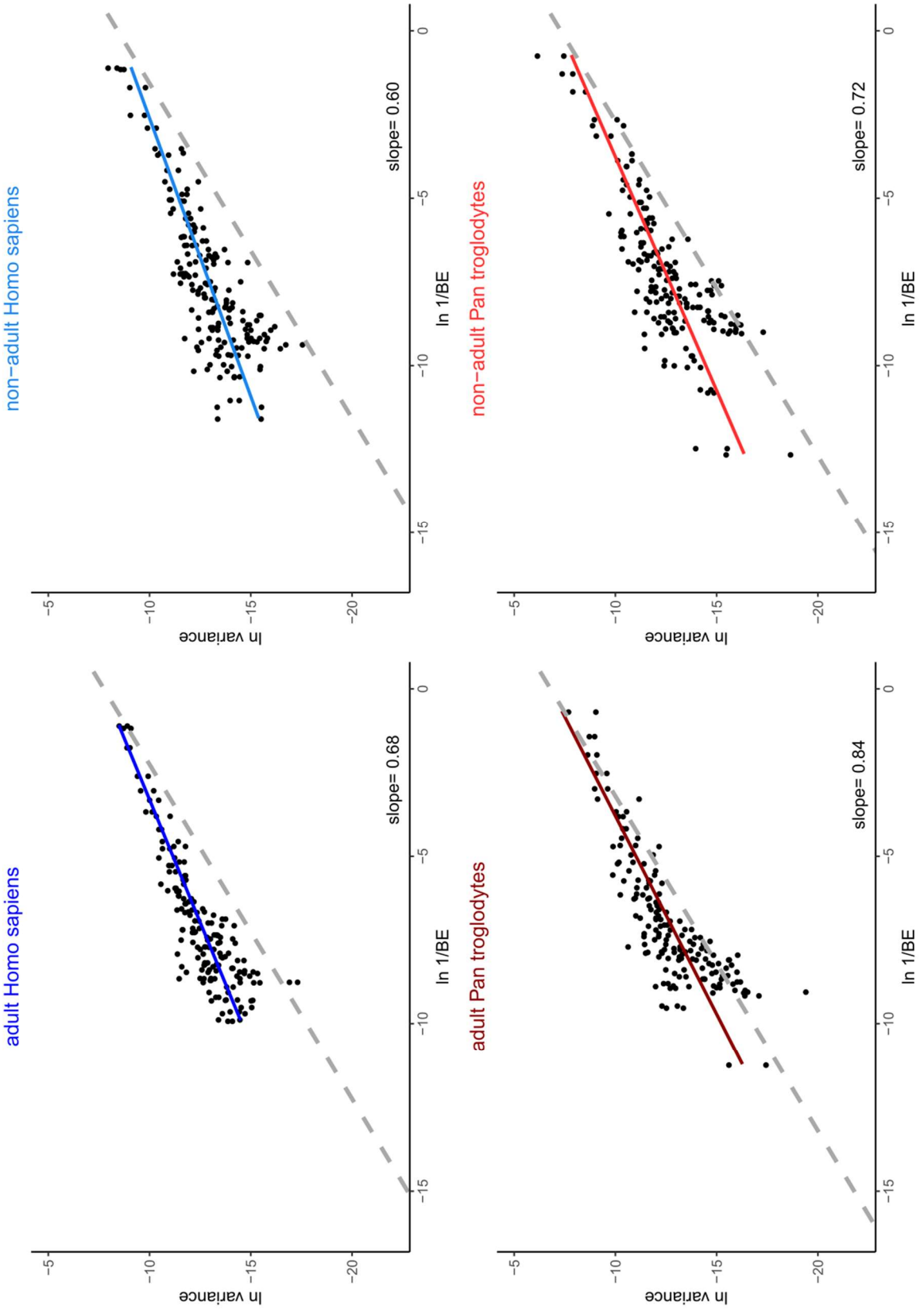

Figure 14. Scatterplots for the linear regression models of log-transformed partial warp variance onto log-transformed inverse bending energy. The grey dotted line indicates a reference regression line with slope=1 and the same intercept as the respective regression model.

Chondrocranium

As for overall cranial shape, the variances of the individual components of the chondrocranium are also high compared to the variance of the overall chondrocranium (see **Table 10** and **Figure 15**). In addition, there is considerable shape variability of the ethmoid bone in the non-adult samples, which is less pronounced in the adult individuals. An increased variance of the sphenoid shape can be seen in all four sample groups.

The linear regressions of the log-transformed partial warp variance onto the log-transformed inverse bending energy yield slopes considerably below 1 (ranging from 0.54 to 0.71) in all sample groups (see **Figure 16**). Furthermore, the regression slopes are lower in the non-adult than in the adult samples.

Table 10. Detailed results for shape variance analysis for the chondrocranium in all sample groups. Summed variances of the individual bones are larger than the variances of the chondrocranium.

	shape variance			
bone	*adult human*	*non-adult human*	*adult chimpanzee*	*non-adult chimpanzee*
occipital	0.0048	0.0028	0.0063	0.0062
basioccipital	0.0143	0.0036	0.0100	0.0038
sphenoid	0.0210	0.0384	0.0203	0.0239
ethmoid	0.0220	0.0639	0.0176	0.1008
sum of variances	0.0620	0.1086	0.0542	0.1345
outline	0.0029	0.0031	0.0038	0.0065

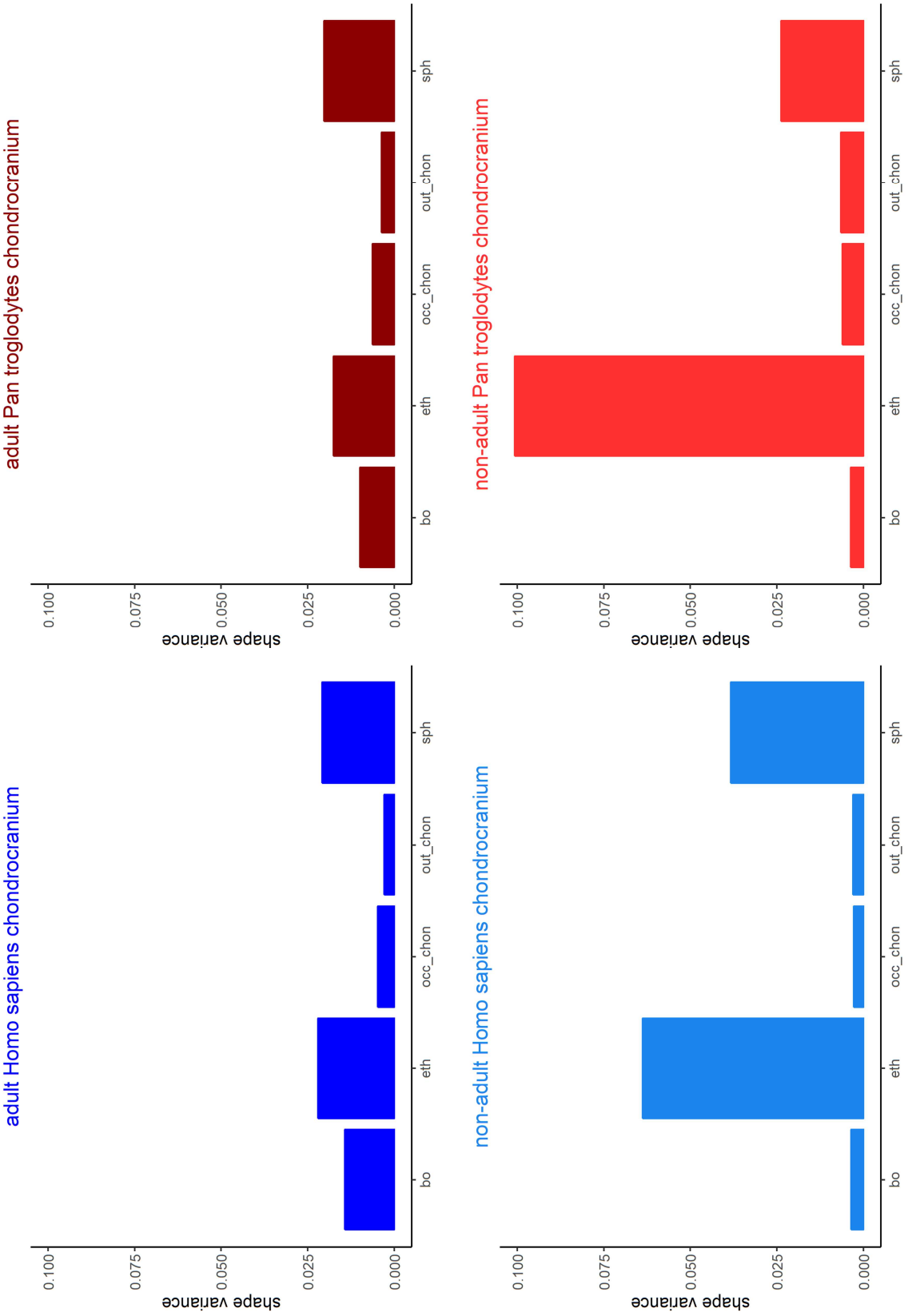

Figure 15. Barplots for the analysis of shape variance in the chondrocranium for all sample groups. Note that, overall, shape, especially of the ethmoid, is more variable in non-adult than in adult individuals. (bo=basioccipital, eth=ethmoid, occ=occipital bone, out_chon=condrocranium, sph=sphenoid)

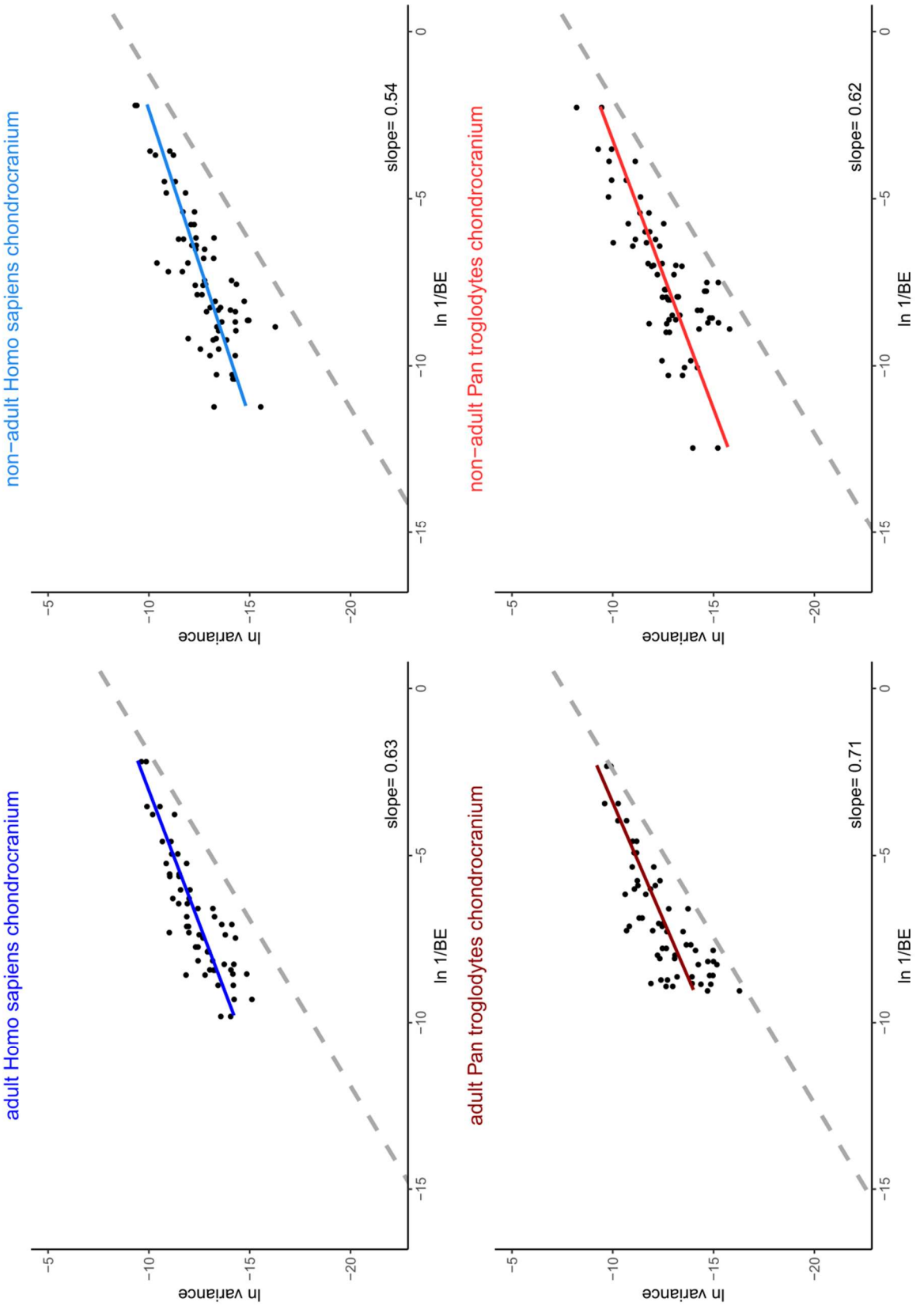

Figure 16. Scatter plots for the linear regression models of log-transformed partial warp variance onto log-transformed inverse bending energy for the chondrocranium. The grey dotted line indicates a reference regression line with slope=1 and the same intercept as the respective regression model.

Desmocranium

The shape variances for the individual bones are high compared to the variance of overall desmocranial shape in all groups (see **Table 11** and **Figure 17**). Further on, small bones, such as the palatine bone, show larger variation than larger bones, such as the frontal bone. **Figure 18** shows that the linear regression slopes of partial warp variance on inverse bending energy for the human samples (non-adults: slope=0.71; adults: slope=0.73) are substantially lower than in either chimpanzee sample (non-adults: slope=0.90; adults: slope=0.94). The slopes of both chimpanzee samples are close to 1 and thus approach the "null-model" of self-similarity.

Table 11. Detailed results for shape variation analysis for the desmocranium. The summed variances of the individual bones are considerably higher than the variances of the overall desmocranium.

	shape variance			
bone	*adult human*	*non-adult human*	*adult chimpanzee*	*non-adult chimpanzee*
parietal	0.0017	0.0008	0.0021	0.0029
vomer	0.0216	0.0164	0.0162	0.0145
premaxilla	0.0396	0.0377	0.0122	0.0206
maxilla	0.0302	0.0292	0.0250	0.0240
palatine	0.0668	0.0321	0.0426	0.0614
nasal	0.0428	0.0495	0.0221	0.0418
frontal	0.0034	0.0025	0.0044	0.0117
sum of variances	0.2061	0.1682	0.1245	0.1769
outline	0.0029	0.0031	0.0038	0.0065

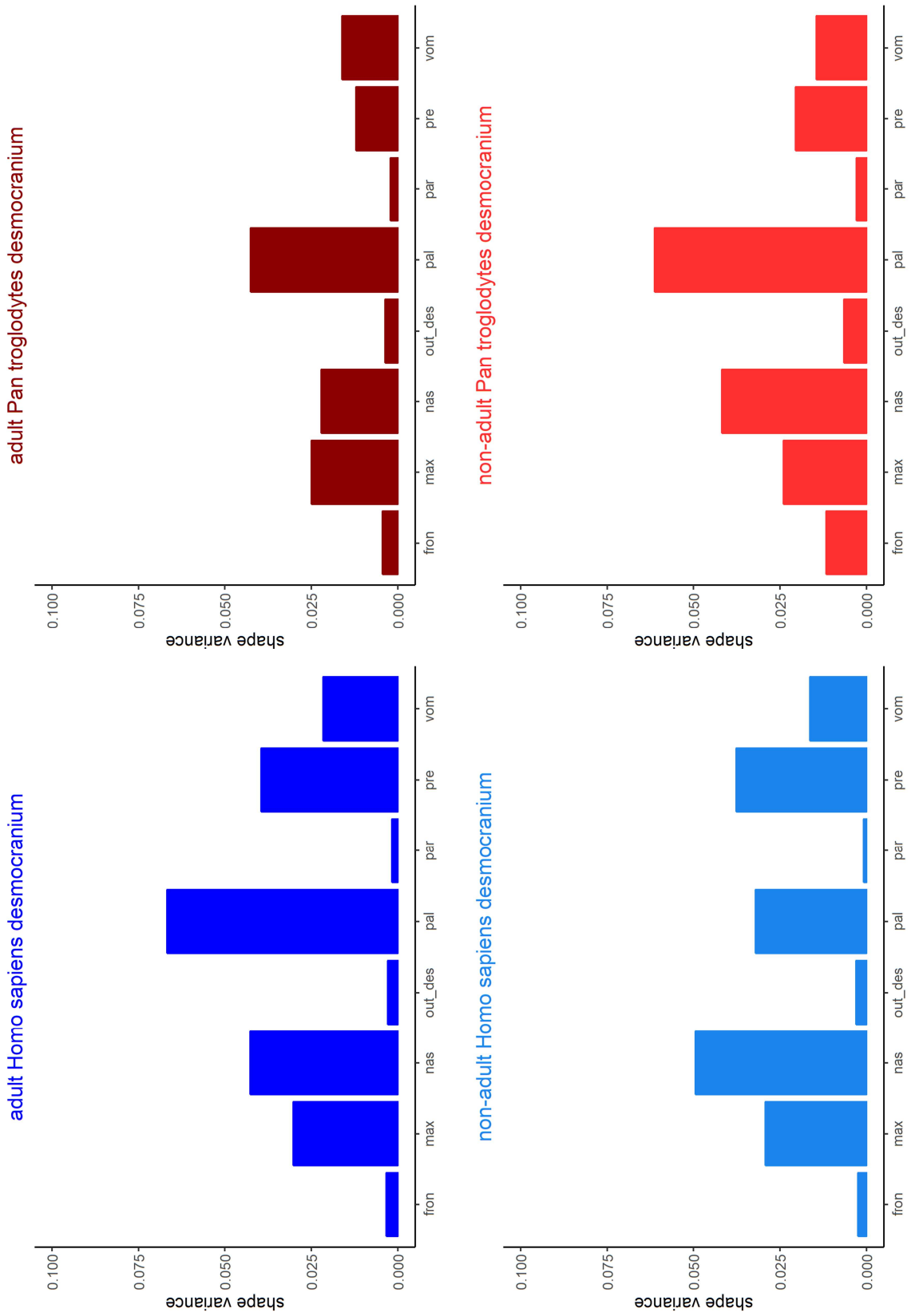

Figure 17. Barplots for the analysis of shape variance in the desmocranium for all sample groups. The increased variance of small bones such as the palatine, the premaxilla and the nasal bone is apparent in all groups. (fron=frontal bone, max=maxilla, nas=nasal bone, out_des=desmocranium, pal=palatine bone, par=parietal bone, pre=premaxilla, vom=vomer)

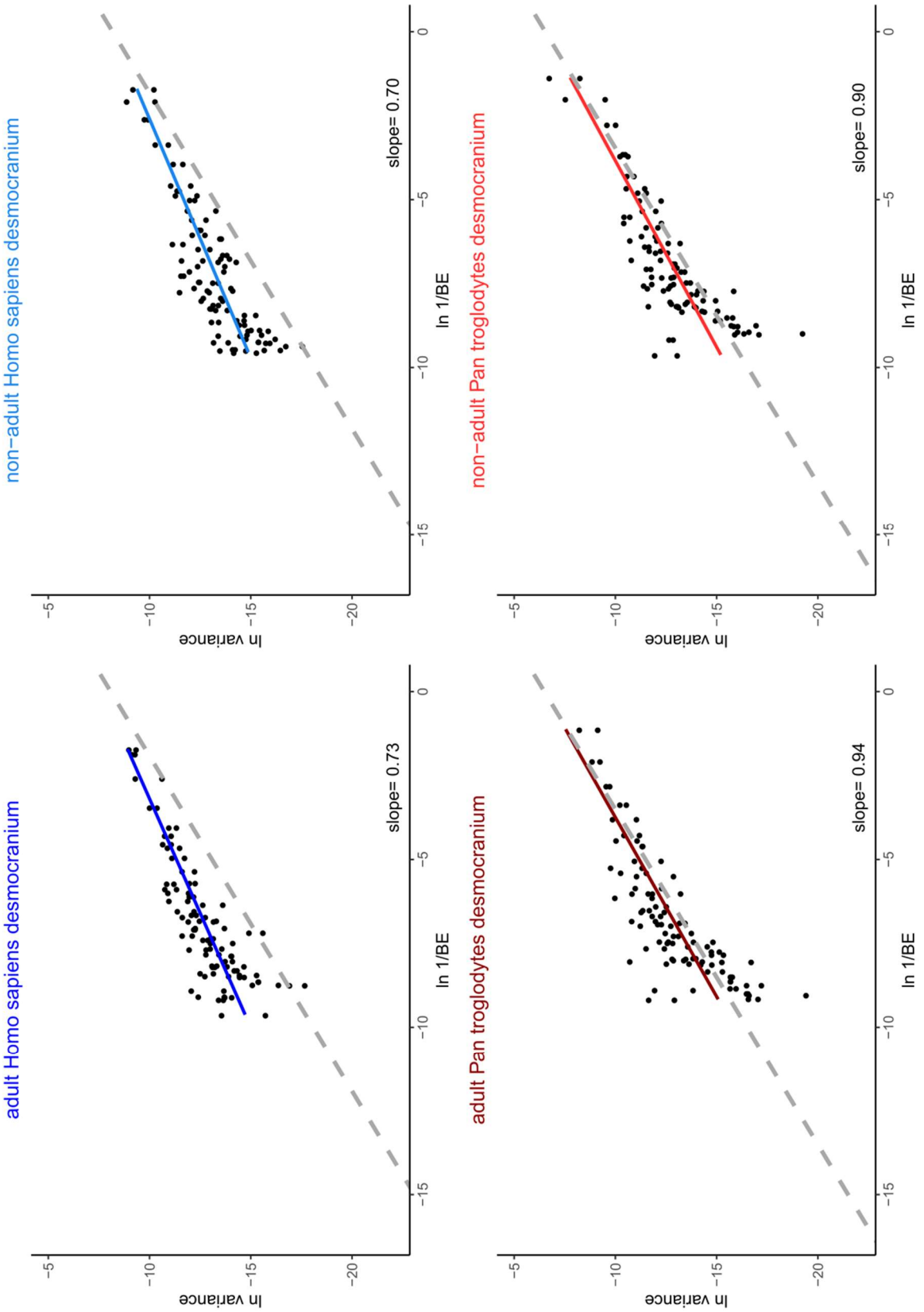

Figure 18. Scatter plots for the linear regression models of log-transformed partial warp variance onto log-transformed inverse bending energy. The increased slope of the chimpanzee groups is clearly visible. The grey dotted line indicates a reference regression line with slope=1 and the same intercept as the respective regression model.

Comparison of global and local shape components

Based on the global shape, i.e. the Procrustes-fitted outline landmark subset, adult chimpanzees are 36% more variable than adult humans.

After standardization of the residual cranial shape in adult *H. sapiens* and adult *P. troglodytes* against the global mean outline shape of both species, chimpanzees are 62% more variable than humans. The results of these calculations can be seen in **Figure 19**.

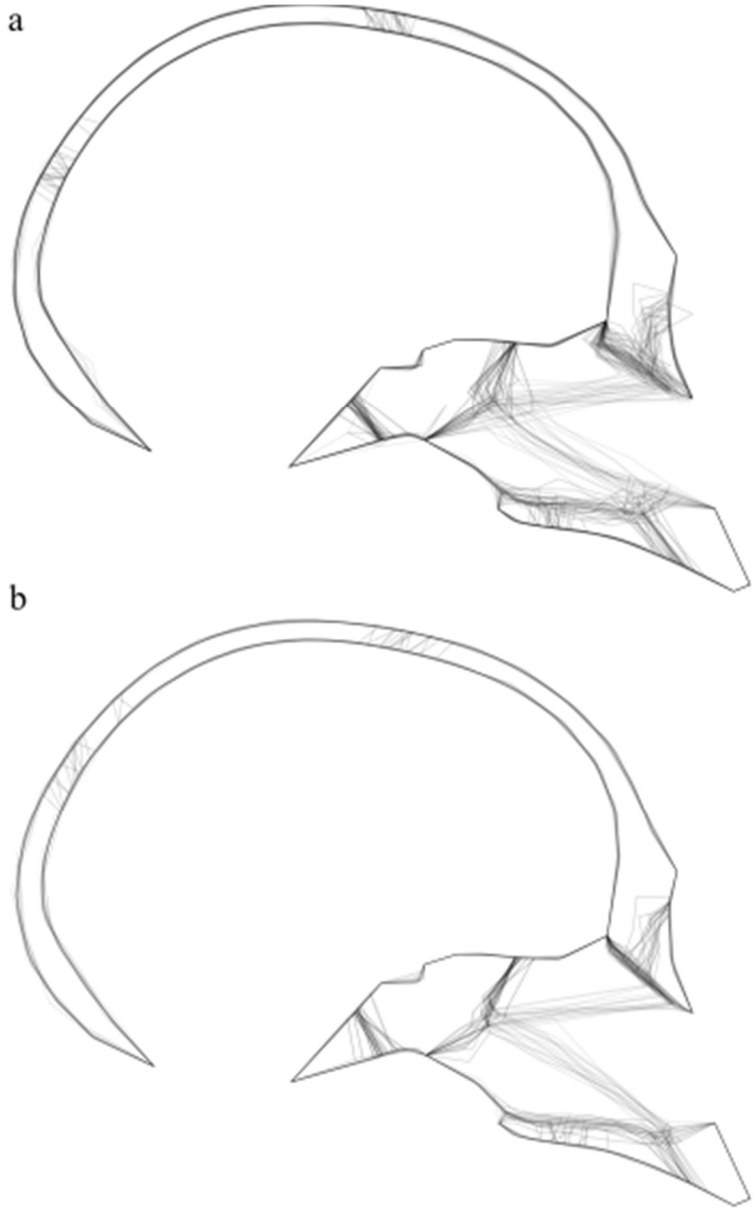

Figure 19. The residual shape of the adult human (a) and chimpanzee (b) sample warped to the mean overall shape of adult chimpanzees and adult humans. The thin lines represent the standardized residual shapes of the individual bones.

A PCA on global shape (i.e. “outline shape”, see **Figure 20a**) shows that the first principal component includes information on both ontogenetic as well as inter-specific shape differences, while the second principal component mainly differentiates between ontogenetic stages. Also, along PC1, adult human specimens are closely followed by non-adult chimpanzees, with hardly any overlap.

By contrast, the first two principal components of the residual shape (**Figure 20b**) do not show as clear a differentiation: Although the residual shape is significantly different between humans and chimpanzees ($p<0.001$), there is no clear differentiation between age stages. Therefore, the main signal of PC1 and PC2 is an inter-specific difference between the sample groups.

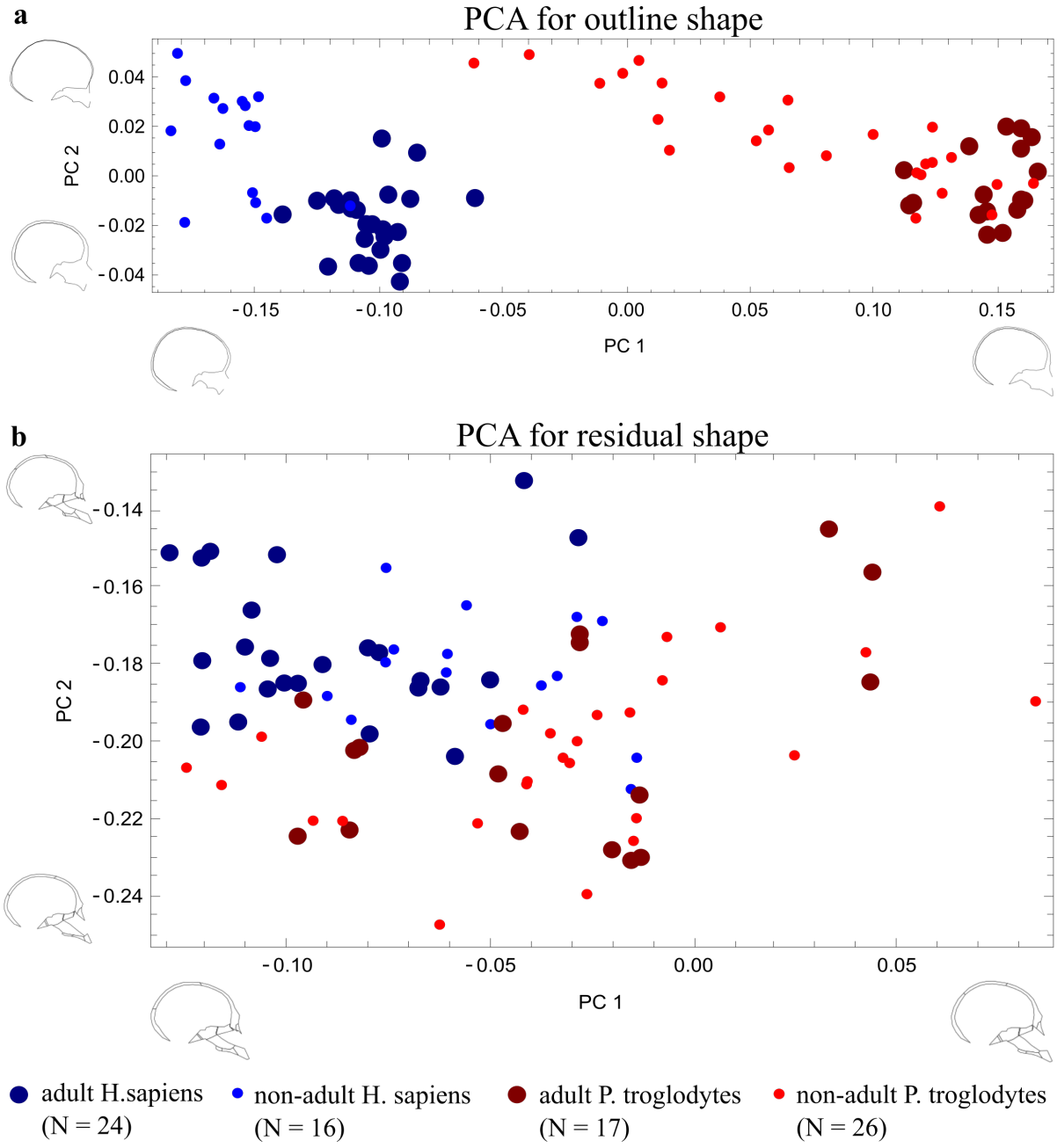

Figure 20. PCA-plots for outline (a) and residual (b) shape of humans and chimpanzees. While ontogenetic trajectories are clearly visible in the outline shape for both species, there is no clear ontogenetic difference in either species in residual shape.

Discussion

The aim of the present thesis was to analyze cranial growth in hominids, more specifically in *H. sapiens* and *P. troglodytes*, and to explore how overall cranial form is established throughout development. As part of this, the present work also compared the shape patterns of the chondrocranium and the desmocranium, in order to infer if different processes underlie the ontogeny of the cranium depending on the type of ossification. A large body of previous morphological work interpreted the presence or absence of covariation in geometric morphometric data as an indicator for the presence or absence of integrated growth processes (Klingenberg & Zaklan, 2000; Klingenberg, 2008; Mitteroecker 2009; Mitteroecker et al. 2012; Neaux, 2017). However, covariances among measurement points, i.e. landmarks, do not necessarily imply interactions during development. For example, the covariance of two spatially adjacent landmarks would necessarily be high, a phenomenon known as *Pearson´s rule of neighborhood* (Whiteley and Pearson, 1899, as cited in Mitteroecker et al., 2012). Therefore, a new method for studying integration has to allow for biologically meaningful interpretations. To this end, a conceptual framework outlined by Bookstein (2015) and Mitteroecker et al. (2019, under review) was implemented to investigate these developmental mechanisms. This approach uses the concept of *self-similarity* as a null model, interpreted as the absence of developmental interactions between components (e.g. cranial bones) of an anatomical structure (e.g. the cranium). The aforementioned conceptual framework further specifies the ways in which deviations from the state of self-similarity point to a dominance of coordinated and compensatory growth processes.

Cranial size

Similar to the results presented by Matiasch (2015) and Mitteroecker et al. (2019, under review), it was found that cranial size is realized through an excess of coordinated growth processes over compensatory ones in both humans and chimpanzees, across both sampled age classes as well as in the desmocranium and the chondrocranium. In all analyses, non-adults of humans and chimpanzees showed a stronger tendency towards coordinated size development of cranial bones than the adult groups. The increased degree of coordinated growth in non-adult individuals is most likely explained by the high variability of size across early ontogenetic stages. Additionally, the adult chimpanzee sample showed the lowest degree of coordinated growth.

Biological interpretation

Coordinated control in the development of size is often necessary to ensure a specific function: For example, a larger mandible has to grow in coordination with a larger maxillary bone in order to allow optimal occlusion. This common control could either be realized by shared developmental timing and growth rates (Mitteroecker et al., 2012), simultaneous, i.e. coordinated, molecular signaling cascades across different tissues or by the expression of pleiotropic genes, which have similar effects in different regions of a developing structure. Examples for these genes include loci encoding bone morphogenic proteins (BMPs), human growth hormone (HGH), several classes of transforming growth factor beta (TGF-β) (Opperman, 2000) or male-specific Y-chromosomal loci (Kirsch et al., 2002) . Another important factor in the coordination of size of the cranium is the growth of the brain. It has an indirect effect on the development of the calvarium through the dura mater, a membrane of connective tissue surrounding the brain. This protective tissue stays in close contact with both the brain and the skull cap. Opperman et al. (1996) found that the dura mater regulates the closure of sutures through the excretion of so-called heparin-binding factors, which act as osteoinhibitors. The sutures are kept unfused during the growth of the brain, therefore facilitating further growth of the calvarium. Once the brain has reached about 90% of the adult size at approximately four (chimpanzees) and five (humans) years of age (Robson & Wood, 2008), growth of the calvarium halts.

Exceptions

An apparent absence of coordinated growth (slope=0.959) was found in the chondrocranium of adult chimpanzees. A possible explanation for the adult chimpanzee case may be that the development of size in chimpanzees is indeed less variable, i.e. more canalized, compared to that of humans. An additional explanation to this finding may be that measurement errors during the course of the landmark setting may result in a self-similar-like pattern: For example, inaccurate measurement of the basioccipital bone would introduce high variance, which may overshadow any size-related covariations between it and the ethmoid bone. These measurement errors would be caused by the obliteration of synchondroses through the growth of sphenoidal sinuses in the chondrocranium, making it difficult to identify bone delineations on CT-scans. Therefore, no definitive conclusions should be drawn from this analysis for adult *P. troglodytes*.

Cranial shape

The shape development of the overall cranium, as well as the chondrocranium, was found to be dominated by compensatory growth processes. This finding could be replicated for *H. sapiens* and *P. troglodytes*, as well as across all age groups, while compensatory growth processes were particularly high in the chondrocranium and in the non-adult groups. In addition, smaller bones, for example the nasal, palatine or premaxillary bone, were generally found to be more variable in terms of shape than larger bones, such as the frontal or parietal bone. Considerable shape variability was found in the ethmoidal bone of non-adult individuals of both chimpanzees and humans. This finding could be explained by the developmental timing of the ethmoid, which is not fully developed until early adulthood.

Biological interpretation

Compensatory growth processes in cranial shape development may be caused by genetic, as well as epigenetic, effects, which canalize cranial growth towards a specific shape, thus giving rise to the signal of compensatory growth processes. Siegal & Bergman (2002) as well as Zelditch et al. (2006) highlighted that, contrary to the common assumption that canalized phenotypes would evolve through long-term selection of an optimal phenotype, developmental processes underlying these phenotypes pose a more likely and easier to evolve way of canalizing traits. Thus, it is assumed that numerous epigenetic effects have a strong influence on cranial shape (e.g. Hallgrímsson et al., 2007, Hall, 2015). One of the most influential concepts for the explanation of epigenetic effects on bone growth is the so-called bone mechanostat model: Bone tissue, being a load carrying material, can only sustain a certain amount of force acting upon it above its typical peak voluntary mechanical load ("the largest repeated and intentional load on bones exerted by intentional activities", see Frost (2003), page 2) before the load eventually exceeds the bones maximum load bearing capacity, resulting in fractures. As a response to continually changing peak loads, a feedback mechanism continuously monitors bone mass and assesses whether it is sufficient to withstand the amount of strain it may experience (Frost, 1996). If bone mass needs to be increased due to a permanently higher mechanical load on the bone, osteocytes signal to osteoblasts to form bone. If, however, there is a reduced need for bone thickness, osteoclasts will reduce bone mass. Similar mechanisms work on the developing cranial bones as a response to variation in the ossification of different bones, resulting in different strains in surrounding regions. For example, if one bone exerts high pressure on adjacent bones, e.g. via increased growth activity, the latter may react through osteoclast activity and therefore bone resorption. Similarly, in the

case of reduced bone growth, the surrounding tissue would experience tension, resulting in increased osteoblast activity and therefore increased bone formation.

An interpretation of the finding that the degree of compensatory growth is especially high in the chondrocranium may be drawn from studies such as that by Lieberman, Pearson and Mowbray (2000). Lieberman and colleagues argued that the cranial base is one of the central integrators of the vertebrate cranium. Most of the basicranial bones undergo chondral ossification and are therefore part of the chondrocranial component in the current work. If the cranial base is indeed a key region for the integration of cranial form, it would need to respond to the shape (and size) variation of both the neurocranium, and the viscerocranium, i.e. facial bones. This assumption is in line with Jeffery and Spoor (2004), who argued that the flexion of the cranial base, itself dependent on bone remodeling processes, may relate to the differential timing of ossification of the desmocranium and the chondrocranium. The present findings on chondrocranial shape are consistent with the hypothesis that the chondrocranium plays a central role during the canalization of hominid cranial form.

Exceptions

An unexpected result was obtained in the analysis of the desmocranium. Whereas non-adult as well as adult human desmocranial shape show an excess of compensatory growth processes over coordinated ones, the chimpanzee desmocranium shows a different growth pattern. Both in the non-adult and in the adult sample, there is no persuasive evidence indicating that compensatory growth processes dominate the development of desmocranial shape in the chimpanzee. Similar to chondrocranial size in adult chimpanzees, measurement error may be responsible for the near self-similar chimpanzee desmocranial shape: According to Cray and colleagues (2008) and Cray, Mooney, and Siegel (2010), the closure of cranial sutures in chimpanzees is associated with the eruption of the third molars and increased masticatory forces experienced by adult individuals. Therefore, adult chimpanzees show a high degree of suture closure, making the reliable measurement of bone delineations increasingly difficult with age. Again, small associations between bones can be obliterated by relatively larger measurement error.

Overall, the above presented results indicate that there is a certain degree of canalization in the development of cranial shape, thus supporting the results of Matiasch (2015): The ontogeny of cranial shape depends on compensatory growth processes, indicating the need to develop functionally relevant cranial shape by counteracting developmental disturbances.

In addition, the comparison of the chondrocranial and desmocranial shape may point towards an additional buffering mechanism of the chondrocranium to shape variability of the desmocranium.

Global and local components of cranial shape

Furthermore, a novel decomposition of global and local components of cranial shape was used in order to test whether the relative contribution of cranial bones to the overall cranium differs between *H. sapiens* and *P. troglodytes*, and whether there are changes in the contribution of bones during ontogeny. The global shape component merely represents the outline shape of the cranium. Firstly, a set of landmarks that delineate the outline of the cranium was defined. By treating type 1 landmarks (landmarks that define borders between tissues, for example sutures), as semilandmarks, and keeping type 2 landmarks (landmarks at extreme points of the cranial outline) fixed, all information on the delineation of bones got eliminated. The local component of cranial shape, on the other hand, captures residual shape changes, i.e. the relative contribution of bones to the overall shape, which was obtained by warping the full set of landmarks to the mean outline shape by thin plate spline interpolation.

The analysis showed that global shape develops along an ontogenetic trajectory: There is a clear separation between age groups, as well as between *H. sapiens* and *P. troglodytes*. These trajectories were found to be largely similar to the ones presented by studies such as Mitteroecker et al. (2004), Mitteroecker et al. (2005) as well as Neubauer et al. (2010), who found "shared aspects of ontogenetic patterns of shape change for most of the postnatal period" (Neubauer et al., 2010, p. 562).

On the other hand, the residual shape did not show clear differences between age stages. There was considerable overlap between non-adult and adult individuals of both species. Species differences were also strongly reduced compared to global shape, although the shape differences between humans and chimpanzees remained statistically significant. Since residual, i.e. local, shape apparently does not undergo considerable postnatal shape change, the relative contribution of bones to overall shape appears to be largely be determined prenatally, in the cartilaginous precursors of bones that undergo chondral ossification. Hall (2015) suggested that prenatal "condensation (of ossification centers) specifies the basic shape and size of skeletal elements, with mechanical forces […] also playing important roles" (p. 321). Moreover, postnatal bone growth seems to be relatively homogenous.

Based on these findings, the cranial shape of humans and chimpanzees, as well as interspecific differences in cranial shape, seems to be accrued globally, rather than through local shape variation. Further on, global features, in contrast to more localized features, of cranial shape are canalized and thus likely functionally more relevant than the relative extent of bones within these structures.

Evolutionary implications and conclusion

Two distinct kinds of processes in cranial development (coordinated size and compensatory shape development) have evolved as mechanisms of a developmental system to respond to perturbations during ontogeny. In the case of size development, it has previously been shown in humans that body height is highly dependent on environmental influences during ontogeny, especially during early childhood: Under ideal circumstances, individuals may reach their full potential in body height, whereas prolonged periods of environmental stress (such as malnutrition and disease) may result in reduced body heights of adult individuals (Grupe et al., 2012). To ensure an organisms functional integrity, these growth retardations have to be under coordinated control, not only within the cranium, but throughout the whole organism and across tissues. If growth of individual bones is uncoordinated, differences in allometric relationships of bones may severely compromise the shape of anatomical structures. The relative consistency and canalization of shape (see below) is thus dependent on the stabilization of body proportions through consistent allometric relationships within a population. As mentioned above, the mechanisms behind size coordination may involve the coordinated expression of genes with pleiotropic effects (e.g. Y-chromosomal growth-control gene (GCY) controlling prolonged growth in males, Kirsch et al., 2002) or the coordinated release of hormones (e.g. somatotropin). The comparison of chimpanzee and human size development revealed only minor differences, mostly in the pattern observed in adult individuals. In terms of the underlying genetics, it has previously been assumed that the growth hormone (GH) locus differs between the two genera in the pattern of gene conversion (Perez-Maya et al., 2012). The morphological effects of these genetic differences remain unclear, but may, at least partly, explain the interspecific differences found in the cranium of adult individuals.

Intraspecific differences regarding the development of global features of cranial shape are established via epigenetic processes, such as the bone mechanostat mechanism and masticatory influences. These processes can be seen as an imminent response of the organism to developmental perturbations. Examples of the reaction to perturbations in shape development via epigenetic processes include fluctuating asymmetry (Hallgrimsson, 1999), which describes

the distribution of asymmetry of a bilaterial organism over developmental time. *Interspecific* differences in the establishment of global shape may have also arisen through epigenetic processes that shape the cranium according to the functional needs of the respective species. However, these epigenetic processes might have manifested themselves in complex genetic networks, for example in those with pleiotropic effects on the condensation of cartilaginous bone precursors. Pavlicev & Wagner (2012) have elaborated on the importance of compensatory changes in the architecture genetic networks underlying complex developmental programs, such as that which controls the development of the cranium.

Regarding the evolutionary changes happening in the local features of cranial shape, it remains to be tested whether the observed differences in local shape between chimpanzees and humans can be explained solely by genetic drift. This finding would imply that the relative contribution of bones to more global anatomical features is indeed comparatively functionally less relevant. Future studies may test this hypothesis. If supported by empirical evidence, the analysis of local shape features may open up new possibilities for morphology-based phylogenetic reconstructions.

References

Albertson, R. C., Streelman, J. T., Kocher, T. D., & Yelick, P. C. (2005). Integration and evolution of the cichlid mandible: the molecular basis of alternate feeding strategies. *Proceedings of the National Academy of Sciences*, *102*(45), 16287-16292.

Armbruster, W. S., Pélabon, C., Bolstad, G. H., & Hansen, T. F. (2014). Integrated phenotypes: understanding trait covariation in plants and animals. *Philosophical Transactions of the Royal Society B: Biological Sciences*, 369(1649).

Bookstein, F. L. (1989). Principal warps: Thin-plate splines and the decomposition of deformations. *IEEE Transactions on pattern analysis and machine intelligence*, 11(6), 567-585.

Bookstein, F. L. (1991, July). Thin-plate splines and the atlas problem for biomedical images. In *Biennial International Conference on Information Processing in Medical Imaging* (pp. 326-342). Springer, Berlin, Heidelberg.

Bookstein, F. L. (2015). Integration, disintegration, and self-similarity: characterizing the scales

of shape variation in landmark data. *Evolutionary biology*, 42(4), 395-426.

Bookstein, F. L. (2018). *A course in morphometrics for biologists: Geometry and statistics for studies of organismal form*. Cambridge University Press.

Bookstein, F. L., Gunz, P., Mitteroecker, P., Prossinger, H., Schaefer, K., & Seidler, H. (2003). Cranial integration in Homo: singular warps analysis of the midsagittal plane in ontogeny and evolution. *Journal of Human Evolution*, 44(2), 167-187.

Cray Jr, J., Meindl, R. S., Sherwood, C. C., & Lovejoy, C. O. (2008). Ectocranial suture closure in Pan troglodytes and Gorilla gorilla: pattern and phylogeny. *American Journal of Physical Anthropology: The Official Publication of the American Association of Physical Anthropologists*, 136(4), 394-399.

Cray Jr, J., Mooney, M. P., & Siegel, M. I. (2010). Timing of ectocranial suture activity in Pan troglodytes as related to cranial volume and dental eruption. *The Anatomical Record: Advances in Integrative Anatomy and Evolutionary Biology*, 293(8), 1289-1296.

Frost, H. M. (1996). Perspectives: A proposed general model of the "mechanostat"(suggestions from a new skeletal-biologic paradigm). *The Anatomical Record: An Official Publication of the American Association of Anatomists*, 244(2), 139-147.

Frost, H. M. (2003). Bone's mechanostat: a 2003 update. *The Anatomical Record Part A: Discoveries in Molecular, Cellular, and Evolutionary Biology: An Official Publication of the American Association of Anatomists*, 275(2), 1081-1101.

Gower, J. C. (1975). Generalized procrustes analysis. *Psychometrika*, 40(1), 33-51.

Grupe, G., Christiansen, K., Schröder, I., & Wittwer-Backofen, U. (2012). Anthropologie: Einführendes Lehrbuch. Springer-Verlag.

Hall, B. K. (2005). Bones and cartilage: developmental and evolutionary skeletal biology. Elsevier.

Hallgrímsson, B. (1999). Ontogenetic patterning of skeletal fluctuating asymmetry in rhesus macaques and humans: evolutionary and developmental implications. *International Journal of Primatology*, 20(1), 121-151.

Hallgrímsson, B., Jamniczky, H., Young, N. M., Rolian, C., Parsons, T. E., Boughner, J. C., & Marcucio, R. S. (2009). Deciphering the palimpsest: studying the relationship between morphological integration and phenotypic covariation. *Evolutionary biology*, 36(4), 355-

376.

Hallgrímsson, B., Lieberman, D. E., Liu, W., Ford-Hutchinson, A. F., & Jirik, F. R. (2007). Epigenetic interactions and the structure of phenotypic variation in the cranium. *Evolution & development*, 9(1), 76-91.

Hansen, T. F. (2003). Is modularity necessary for evolvability?: Remarks on the relationship between pleiotropy and evolvability. *Biosystems*, 69(2-3), 83-94.

Jeffery, N., & Spoor, F. (2004). Ossification and midline shape changes of the human fetal cranial base. *American Journal of Physical Anthropology*, 123(1), 78-90.

King, M. C., & Wilson, A. C. (1975). Evolution at two levels in humans and chimpanzees. *Science*, 188(4184), 107-116.

Kirsch, S., Weiss, B., Kleiman, S., Roberts, K., Pryor, J., Milunsky, A., ... & Rappold, G. A. (2002). Localisation of the Y chromosome stature gene to a 700 kb interval in close proximity to the centromere. *Journal of medical genetics*, 39(7), 507-513.

Klingenberg, C. P., & Zaklan, S. D. (2000). Morphological integration between developmental compartments in the Drosophila wing. *Evolution*, *54*(4), 1273-1285.

Klingenberg, C. P. (2008). Morphological integration and developmental modularity. *Annual review of ecology, evolution, and systematics*, 39, 115-132.

Lande, R. (1980). The genetic covariance between characters maintained by pleiotropic mutations. *Genetics*, 94(1), 203-215.

Lewontin, R. C. (1978). Adaptation. *Scientific American*, 239 (1), 156-169.

Lieberman, D. E., McBratney, B. M., & Krovitz, G. (2002). The evolution and development of cranial form in Homo sapiens. *Proceedings of the National Academy of Sciences*, 99(3), 1134-1139.

Lieberman, D. E., & McCarthy, R. C. (1999). The ontogeny of cranial base angulation in humans and chimpanzees and its implications for reconstructing pharyngeal dimensions. *Journal of Human Evolution*, 36(5), 487-517.

Lieberman, D. E., Pearson, O. M., & Mowbray, K. M. (2000). Basicranial influence on overall cranial shape. *Journal of human evolution*, 38(2), 291-315.

Lieberman, D. E., Ross, C. F., & Ravosa, M. J. (2000). The primate cranial base: ontogeny,

function, and integration. *American Journal of Physical Anthropology: The Official Publication of the American Association of Physical Anthropologists*, 113(S31), 117-169.

Marie, P. J., Coffin, J. D., & Hurley, M. M. (2005). FGF and FGFR signaling in chondrodysplasias and craniosynostosis. *Journal of cellular biochemistry*, 96(5), 888-896.

Matiasch, C. (2015). „Developmental control of cranial form: coordinated or compensatory?". Master´s Thesis, University of Vienna.

Mitteroecker, P. (2009). The developmental basis of variational modularity: insights from quantitative genetics, morphometrics, and developmental biology. *Evolutionary biology*, 36(4), 377-385.

Mitteroecker, P., Bartsch, S., Erkinger, C., & Grunstra, N. D. S. (2019). Morphometric Variation at Different Spatial Scales : Coordination and Compensation in the Emergence of Organismal Form. *Under Review.*

Mitteroecker, P., & Bookstein, F. (2008). The evolutionary role of modularity and integration in the hominoid cranium. *Evolution: International Journal of Organic Evolution*, 62(4), 943-958.

Mitteroecker, P., & Gunz, P. (2009). Advances in geometric morphometrics. *Evolutionary Biology*, 36(2), 235-247.

Mitteroecker, P., Gunz, P., Bernhard, M., Schaefer, K., & Bookstein, F. L. (2004). Comparison of cranial ontogenetic trajectories among great apes and humans. *Journal of Human Evolution*, 46(6), 679-698.

Mitteroecker, P., Gunz, P., & Bookstein, F. L. (2005). Heterochrony and geometric morphometrics: a comparison of cranial growth in Pan paniscus versus Pan troglodytes. *Evolution & Development*, 7(3), 244-258.

Mitteroecker, P., Gunz, P., Neubauer, S., & Müller, G. (2012). How to explore morphological integration in human evolution and development?. *Evolutionary Biology*, 39(4), 536-553.

Müller, G. B. (2007). Evo–devo: extending the evolutionary synthesis. *Nature reviews genetics*, 8(12), 943.

Neaux, D. (2017). Morphological integration of the cranium in Homo, Pan, and Hylobates and the evolution of hominoid facial structures. *American journal of physical anthropology*, 162(4), 732-746.

Needham, J. (1933). On the dissociability of the fundamental processes in ontogenesis. *Biological Reviews*, 8(2), 180-223.

Neubauer, S., Gunz, P., & Hublin, J. J. (2010). Endocranial shape changes during growth in chimpanzees and humans: a morphometric analysis of unique and shared aspects. *Journal of human evolution*, 59(5), 555-566.

Olson, E. C., & Miller, R. L. (1958). Morphological integration. University of Chicago Press.

Opperman, L. A. (2000). Cranial sutures as intramembranous bone growth sites. *Developmental dynamics: an official publication of the American Association of Anatomists*, 219(4), 472-485.

Opperman, L. A., Passarelli, R. W., Nolen, A. A., Gampper, T. J., Lin, K. Y., & Ogle, R. C. (1996). Dura mater secretes soluble heparin-binding factors required for cranial suture morphogenesis. *In Vitro Cellular & Developmental Biology-Animal*, 32(10), 627-632.

Ornitz, D. M., & Marie, P. J. (2002). FGF signaling pathways in endochondral and intramembranous bone development and human genetic disease. *Genes & development*, 16(12), 1446-1465.

Pavlicev, M., & Hansen, T. F. (2011). Genotype-phenotype maps maximizing evolvability: Modularity revisited. *Evolutionary Biology*, 38(4), 371-389.

Pavlicev, M., & Wagner, G. P. (2012). A model of developmental evolution: selection, pleiotropy and compensation. *Trends in Ecology & Evolution*, 27(6), 316-322.

Pérez-Maya, A. A., Rodríguez-Sánchez, I. P., de Jong, P., Wallis, M., & Barrera-Saldaña, H. A. (2012). The chimpanzee GH locus: composition, organization, and evolution. *Mammalian genome*, 23(5-6), 387-398.

Rice, S. H. (1997). The analysis of ontogenetic trajectories: when a change in size or shape is not heterochrony. *Proceedings of the National Academy of Sciences*, 94(3), 907-912.

Robson, S. L., & Wood, B. (2008). Hominin life history: reconstruction and evolution. *Journal of Anatomy*, 212(4), 394-425.

Rohlf, F. J., & Slice, D. (1990). Extensions of the Procrustes method for the optimal superimposition of landmarks. *Systematic Biology*, 39(1), 40-59.

Ruvolo, M. (1997). Molecular phylogeny of the hominoids: inferences from multiple

independent DNA sequence data sets. *Molecular biology and evolution*, 14(3), 248-265.

Scott, N. A., Strauss, A., Hublin, J. J., Gunz, P., & Neubauer, S. (2018). Covariation of the endocranium and splanchnocranium during great ape ontogeny. *PloS one*, 13(12), e0208999.

Siegal, M. L., & Bergman, A. (2002). Waddington's canalization revisited: developmental stability and evolution. *Proceedings of the National Academy of Sciences*, 99(16), 10528-10532.

Smith, B. H., Crummett, T. L., & Brandt, K. L. (1994). Ages of eruption of primate teeth: a compendium for aging individuals and comparing life histories. *American journal of physical anthropology*, 37(S19), 177-231.

Strait, D. S. (2001). Integration, phylogeny, and the hominid cranial base. *American Journal of Physical Anthropology: The Official Publication of the American Association of Physical Anthropologists*, 114(4), 273-297.

Waddington, C. H. (1942). Canalization of development and the inheritance of acquired characters. *Nature*, 150(3811), 563.

Wagner, G. P. (1996). Homologues, natural kinds and the evolution of modularity. *American Zoologist*, 36(1), 36-43.

Wagner, G. P., & Altenberg, L. (1996). Perspective: complex adaptations and the evolution of evolvability. *Evolution*, 50(3), 967-976.

Wagner, G. P., Pavlicev, M., & Cheverud, J. M. (2007). The road to modularity. *Nature Reviews Genetics*, 8(12), 921.

White, T. D., & Folkens, P. A. (2005). The human bone manual. Elsevier.

Zelditch, M. L., Bookstein, F. L., & Lundrigan, B. L. (1993). The ontogenetic complexity of developmental constraints. *Journal of Evolutionary Biology*, 6(5), 621-641.

Zelditch, M. L., Lundrigan, B. L., & Garland Jr, T. (2004). Developmental regulation of skull morphology. I. Ontogenetic dynamics of variance. *Evolution & development*, 6(3), 194-206.

Zelditch, M. L., Mezey, J., Sheets, H. D., Lundrigan, B. L., & Garland Jr, T. (2006). Developmental regulation of skull morphology II: ontogenetic dynamics of covariance. *Evolution & development*, 8(1), 46-60.

List of figures

List of tables

Appendix

R-code

Definition of bones

```
parietal<-c(1,5,7,9,11,13,15,3,4,16,14,12,10,8,6,2)
occipital<-c(3,18,20,22,24,26,28,17,29,27,25,23,21,19,4)
occipital_chon<-c(3,18,20,22,24,26,28,17,29,27,25,23,21,19,4)
basioccipital<-c(30,31,39)
gap_bo_sph<-c(31,32,40,39)
sphenoid<-c(32,33,34,35,36,37,46,44,42,43,38,41,40)
gap_sph_eth<-c(46,47,45,42,44)
vomer<-c(53,54,55,42,43,38,60,59,69,67,65,63,61)
ethmoid<-c(47,48,49,91,93,51,42,45)
premaxilla<-c(52,56,57,62,61,53)
maxilla<-c(61,63,65,67,68,66,64,62)
palatine<-c(67,69,59,58,70,68)
gap_eth_fr_nas<-c(50,92,76,51,93,91,49)
nasal<-c(72,73,71,77,76,75,74)
frontal<-c(1,89,87,85,83,81,79,78,72,74,75,76,92,50,80,82,84,86,88,90,2)
outline1<-
c(1,5,7,9,11,13,15,3,18,20,22,24,26,28,17,29,27,25,23,21,19,4,16,14,12,10,8
,6,2,90,88,86,84,82,80,50,49,48,47,46,37,36,35,34,33,32,31,30,39,40,41,38,6
0,59,58,70,68,66,64,62,57,56,52,71,73,72,78,79,81,83,85,87,89)
chondrocranium<-
c(3,4,17,18,19,20,21,22,23,24,25,26,27,28,29,30,31,32,33,34,35,36,37,38,39,
40,41,42,43,46,47,48,49,51,91,93)
desmocranium<-
c(1,2,3,4,5,6,7,8,9,10,11,12,13,14,15,16,38,42,43,50,52,53,54,55,56,57,58,5
9,60,62,64,66,68,70,71,72,73,76,77,78,79,80,81,82,83,84,85,86,87,88,89,90,9
2)
```

Calculation of areas

```
library(splancs)
nspec=83 #number of specimens in the array
#exemplary function for the analysis of the overall cranium
bone_areas_splancs<-function(ARRAY){

  summary<-matrix(nrow=nspec,ncol=12)
  colnames(summary)<-
c("par","occ","bo","sph","vom","eth","pre","max","pal","nas","fron","out")
  rownames(summary)<-dimnames(ARRAY)[[3]]

  for (i in 1:dim(ARRAY)[[3]]) {

    areas_i<-matrix(nrow=12,ncol=1)

    a<-as.matrix(ARRAY[,,i])

    areas_i[1,]<-areapl(a[parietal,])
    areas_i[2,]<-areapl(a[occipital,])
    areas_i[3,]<-areapl(a[basioccipital,])
    areas_i[4,]<-areapl(a[sphenoid,])
    areas_i[5,]<-areapl(a[vomer,])
    areas_i[6,]<-areapl(a[ethmoid,])
    areas_i[7,]<-areapl(a[premaxilla,])
```

```
    areas_i[8,]<-areapl(a[maxilla,])
    areas_i[9,]<-areapl(a[palatine,])
    areas_i[10,]<-areapl(a[nasal,])
    areas_i[11,]<-areapl(a[frontal,])
    areas_i[12,]<-areapl(a[outline1,])

    summary[i,]<-areas_i
  }
  return(summary)
}
```

Calculation of bending energy and partial warp scores

```
libray(Morpho)
create partialW be<-
function(ARRAY,m_overall,m_mshape,nspec,mode=c("overall","chondrocranium","
desmocranium")){

  if(mode=="overall"){

    m_L<-CreateL(m_mshape)
    m_kxk<-as.matrix(m_L$Lsubk)
    m_eigen<-eigen(m_kxk)
    m_prinwarps<-m_eigen$vectors
    m_be<-m_eigen$values
    summary<-matrix(nrow = nspec,ncol = dim(m_overall)[[1]]*2)
    rownames(summary)<-dimnames(ARRAY)[[3]]
    m_x <- matrix(NA, nrow = dim(ARRAY)[[3]],ncol = dim(ARRAY)[[1]])
    m_y <- matrix(NA, nrow = dim(ARRAY)[[3]],ncol = dim(ARRAY)[[1]])

    for (i in 1:dim(m_overall)[[3]]){
      m_x[i,]<-m_overall[,1,i]-m_mshape[,1]
      m_y[i,]<-m_overall[,2,i]-m_mshape[,2]

    }

    m_x_PWscores<-m_x%*%m_prinwarps
    colnames(m_x_PWscores)<-paste(1:ncol(m_x),"X")
    m_y_PWscores<-m_y%*%m_prinwarps
    colnames(m_y_PWscores)<-paste(1:ncol(m_y),"Y")
    results<-
list(bendingEnergy=m_be,partialWarps=cbind(m_x_PWscores,m_y_PWscores))
    return(results)
  }

  else if(mode=="chondrocranium"){

    m_L<-CreateL(m_mshape)
    m_kxk<-as.matrix(m_L$Lsubk)
    m_eigen<-eigen(m_kxk)
    m_prinwarps<-m_eigen$vectors
    m_be<-m_eigen$values
    summary<-matrix(nrow = nspec,ncol = dim(m_overall)[[1]]*2)
    rownames(summary)<-dimnames(ARRAY)[[3]]
    m_x <- matrix(NA, nrow = dim(ARRAY)[[3]],ncol = dim(ARRAY)[[1]])
    m_y <- matrix(NA, nrow = dim(ARRAY)[[3]],ncol = dim(ARRAY)[[1]])

    for (i in 1:dim(m_overall)[[3]]){
      m_x[i,]<-m_overall[,1,i]-m_mshape[,1]
      m_y[i,]<-m_overall[,2,i]-m_mshape[,2]
```

```
    }

    m_x_PWscores<-m_x%*%m_prinwarps
    colnames(m_x_PWscores)<-paste(1:ncol(m_x),"X")
    m_y_PWscores<-m_y%*%m_prinwarps
    colnames(m_y_PWscores)<-paste(1:ncol(m_y),"Y")
    results<-
list(bendingEnergy=m_be,partialWarps=cbind(m_x_PWscores,m_y_PWscores))
    return(results)
  }

  else {

    m_L<-CreateL(m_mshape)
    m_kxk<-as.matrix(m_L$Lsubk)
    m_eigen<-eigen(m_kxk)
    m_prinwarps<-m_eigen$vectors
    m_be<-m_eigen$values
    summary<-matrix(nrow = nspec,ncol = dim(m_overall)[[1]]*2)
    rownames(summary)<-dimnames(ARRAY)[[3]]
    m_x <- matrix(NA, nrow = dim(ARRAY)[[3]],ncol = dim(ARRAY)[[1]])
    m_y <- matrix(NA, nrow = dim(ARRAY)[[3]],ncol = dim(ARRAY)[[1]])

    for (i in 1:dim(m_overall)[[3]]){
      m_x[i,]<-m_overall[,1,i]-m_mshape[,1]
      m_y[i,]<-m_overall[,2,i]-m_mshape[,2]

    }

    m_x_PWscores<-m_x%*%m_prinwarps
    colnames(m_x_PWscores)<-paste(1:ncol(m_x),"X")
    m_y_PWscores<-m_y%*%m_prinwarps
    colnames(m_y_PWscores)<-paste(1:ncol(m_y),"Y")
    results<-
list(bendingEnergy=m_be,partialWarps=cbind(m_x_PWscores,m_y_PWscores))
    return(results)
  }

}
```